Volume 18
Number 1

June *2016*
(ISSN 1109-1606)

Journal of APPLIED ELECTROMAGNETISM

JAE

Institute of Communication and Computer Systems

Athens - GREECE

Volume 18 June 2016
Number 1 (ISSN 1109-1606)

JOURNAL
OF
APPLIED ELECTROMAGNETISM

Trans Black Sea Region Union of Applied Electromagnetism

BSUAE

Institute of Communication and Computer Systems

Athens - GREECE

Volume 18 **Number 1**

June 2016

TRANS BLACK SEA REGION UNION OF APPLIED ELECTROMAGNETISM (BSUAE)

JOURNAL OF APPLIED ELECTROMAGNETISM

Institute of Communication and Computer Systems

Athens - GREECE

Editor: Panayiotis Frangos (Greece), pfrangos@central.ntua.gr

Honorary Editor: Nikolaos K. Uzunoglu (Greece), nuzu@central.ntua.gr

Board of Associate Editors

D. Dimitrov (Bulgaria), dcd@tu-sofia.bg
V. Dumbrava (Lithuania), vydum@ktu.lt
G. Georgiev (Bulgaria), gngeorgiev@yahoo.com
G. Matsopoulos (Greece), gmatso@esd.ece.ntua.gr

Editorial Board

ALBANIA
G. Bardhyf, bardhylgolemi@live.com
C. Pirro, p_cipo@yahoo.com

ARMENIA
H. Bagdasarian, hovik@seua.sci.am
H. Terzian, hterzian@seua.sci.am

BULGARIA
A. Antonov, asantonov@abv.bg
A. Lazarov, lazarov@bfu.bg
S. Savov, savovsv@yahoo.com

GEORGIA
R. Zaridze, rzaridze@laetsu.org

GERMANY
M. Georgieva – Grosse, mariana.georgieva-grosse@de.bosch.com

GREECE
H. Anastassiu, ANASTASIOU.Christos@haicorp.com
I. Avramopoulos, hav@mail.ntua.gr
G. Fikioris, gfiki@cc.ece.ntua.gr
J. Kanellopoulos, ikanell@cc.ece.ntua.gr
G. Karagiannidis, geokarag@auth.gr
G. Kliros, gsksma@hol.gr
T. Mathiopoulos, mathio@space.noa.gr
C. Moschovitis, harism@noc.ntua.gr
K. Nikita, knikita@cc.ece.ntua.gr

I. Ouranos, iouranos@central.ntua.gr
E. Papkelis, spapkel@central.ntua.gr
J. Sahalos, sahalos@auth.gr
M. Theologou, theolog@cs.ntua.gr
N. Triantafyllou, nitriant@central.ntua.gr
K. Ksystra, katksy@central.ntua.gr
A. Malamou, annamalamou@yahoo.gr
S. Bourgiotis, sbourgiotis@mail.ntua.gr

JORDAN
N. Dib, nihad@just.edu.jo

KAZAKSHTAN
S. Sautbekov, sautbek@mail.ru

LITHUANIA
L. Svilainis, linas.svilainis@ktu.lt

RUSSIA
M. Bakunov, bakunov@rf.unn.ru
A. Grigoriev, adgrigoriev@mail.ru

SERBIA
B. Reljin, ereljin@ubbg.etf.bg.ac.yu

SPAIN
E. Gago – Ribas, egr@tsc.uniovi.es
M. Gonzalez – Morales, gonmor@yllera.tel.uva.es

UNITED KINGDOM
G. Goussetis, G.Goussetis@hw.ac.uk

Publishing Department

N. Triantafyllou, nitriant@central.ntua.gr
K. Ksystra, katksy@central.ntua.gr
A. Malamou, annamalamou@yahoo.gr
S. Bourgiotis, sbourgiotis@mail.ntua.gr

Journal of Applied Electromagnetism

Copyright Form

The undersigned I confirm that I agree the publication of the article

in the Journal of Applied Electromagnetism and the copyright to belong to Trans Black Sea Union of Applied Electromagnetism. I understand that I have the full right to reuse this manuscript for my own purposes.

Name:

Surname:

Address:

E-mail:

Signed:

***Please send the previous form signed either by e-mail to pfrangos@central.ntua.gr , or by fax to the fax number: +30 210 772 2281, attention of Prof. P. Frangos.**

Address

Institute of Communication and Computer Systems,

National Technical University of Athens,

9, Iroon Polytechniou Str.,

157 73 Athens - GREECE

Tel: (+30) 210 772 3694

Fax: (+30) 210 772 2281, attention of Prof. P. Frangos

e-mail: pfrangos@central.ntua.gr

Web site: **http://jae.ece.ntua.gr**

TRANS BLACK SEA REGION UNION OF APPLIED ELECTROMAGNETISM (BSUAE)

JOURNAL OF APPLIED ELECTROMAGNETISM (JAE)

Volume 18 Number 1 June 2016

CONTENTS

INFLUENCE OF THE WALLS TRANSPARENCY ON THE RESONANT EM FIELD'S VALUES

V. Jeladze, V. Tabatadze, M. Prishvin, I. Petoev, R. Zaridze 1

A mobile communication system base station's radiation interaction with a human model inside of a room in a building is studied in this article. The inner field and its amplification by the walls that in some cases act like a resonator are studied. The problem is solved using the Method of Auxiliary Sources with a user friendly program package, created for numerical experiments for this particular problem. Several cases of the human location and building wall's transparency parameters are considered during the calculations. The numerical experiment results are presented and analyzed.

APPLICATION OF LIMIT RELATIONS METHOD TO THOMSON'S MODEL OF HIGH-FREQUENCY INDUCTIVE DISCHARGEOF FINITE LENTH

A.P. Kirpichnikov 14

The exhaustive analytical solution to the task about the structure of quasistationary electromagnetic field of high-frequency inductive discharge of finite length near the axis of plasma bunch is given.

STUDYING THE EQUATION OF MOTION FOR MAGNETIC FLUIDS WITH NANO-PARTICLE INCLUSIONS (short paper)

K. Kotetishvili, E. Iordanishvili, N. Kobalia, G. Chikhladze 31

The paper deals with investigations of equation of motion for magnetic fluids, consisting of nano-particles or holding definite nano-particle inclusions. The equation is received by means of application the laws of conservation for linear and angular momentums. In low magnetic fields fluids are unable to reach saturation and nano-particles revolve in additional rotating magnetic field. The magnetization in magnetic fluids increases in spiral form.

MULTI-HOP DATA TRANSMISSION IN WSN FOR FREE SPACE ENVIRONMENT

Z. Ganev, S. Savov **37**

This article deals with idealized isotropic model of data transmission in free space environment. This is a model by which data to base station does not arrive directly, but by the means of multi-hop method. Thus data transmission energy is considerably reduced and network life is prolonged , which is a main task of many designer. We have four different examples, which illustrate how the transmission energy can be significantly reduced. The energy model is simulated with Matlab and results visualized with appropriate graphics.

INFLUENCE OF THE WALLS TRANSPARENCY ON THE RESONANT EM FIELD'S VALUES

V. Jeladze, V. Tabatadze, M. Prishvin, I. Petoev, R. Zaridze

Tbilisi State University, Laboratory of Applied Electrodynamics and Radio Engineering

3, Chavchavadze Ave. Tbilisi, Georgia

Email: veriko.jeladze001@ens.tsu.edu.ge, Email: prishvin@gmail.com,

Email: revaz_zaridze@mail.ru

Abstract

A mobile communication system base station's radiation interaction with a human model inside of a room in a building is studied in this article. The inner field and its amplification by the walls that in some cases act like a resonator are studied. The problem is solved using the Method of Auxiliary Sources with a user friendly program package, created for numerical experiments for this particular problem. Several cases of the human location and building wall's transparency parameters are considered during the calculations. The numerical experiment results are presented and analyzed.

1. INTRODUCTION

In our previous works the mobile phone antenna radiation influence on the user's body has been considered when the user was located inside the room while talking over the mobile phone. As the numerical experiments showed, in some cases, the room behaves as a resonator and amplifies the antenna radiated field. The field value may be amplified and becomes dangerous for the user [1]. In this article our goal is to investigate the case when an EM source is located outside of the building, particularly, it is the base station antenna. The human model is located in a fixed place inside of a room with a window and as it is show later its position is of a big importance. A homogenous dielectric model of a human shape "Mummy" [1] has been used in numerical experiments. Tissues parameters are averaged since their inhomogeneity does not affect the final results significantly. Base station has the pretty high intensity radiation, if the

room is nearby, the field which goes inside of the room is may be amplified because if the resonant effects of the room. Usually, when the radiation safety standards are established and fulfilled the fields have to be safe for humans, the responsible personal measure the field, bud usually it happens outside of the building. But when such measurements are conducted, the resonant properties of a room are not taken into account, which in some cases amplifies the field and may produce health hazard. In frames of this article we would like to show that in order to determine how far the base station antenna should be located, the mentions properties of a building have to be studied carefully.

In the article [1] a detailed investigation and a justification of a possibility to use a homogenous dielectric human shaped body "Mummy" with constant averaged permittivity and losses values (frequency dependent) instead of inhomogeneous human issues are presented. The use of such model is needed to implement the Method of Auxiliary Sources for calculations diffraction problems on human model as well as on big scenarios like room.

The numerical calculations have been conducted based on FDTD method in [2] for the inhomogeneous child and a woman voxel models from virtual family. The frequencies used were 300 MHz, 1900 MHz and 3700 MHz and a dipole antenna as an EM source. In our earlier studies [3] we have considered only a room without a human model. The frequency was not higher than 400 MHz because the computer resources at that time were not enough to study real case scenarios. It was noted, that on some resonant frequencies the standing wave arise which must depend on walls transparency.

In this study we consider a room with various walls transparency and a homogeneous human model inside at frequencies nearby 900 MHz. It is important to take into account the possible resonant effects and study SAR distributions for such cases more carefully.

2. THE PROBLEM STATEMENT AND MATHEMATICAL APPROACH

The stated problem corresponds to the study of the diffraction of the harmonic EM wave field on a homogenous dielectric object with the shape shown on figure 1, which is located inside of the semi open surface like room. As the base station's EM field's source we consider a combined dipole with definite amplitude, located outside of the room. The

problem is solved by means of the Method of Auxiliary Sources (MAS) which gives ability to solve efficiently complicated and big scenarios with minimal CPU usage [2].

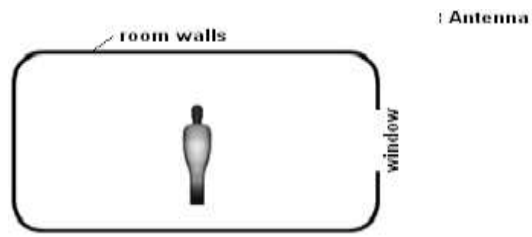

Figure 1. Model geometry

Application of the MAS is deduced to the construction of two couples of closed auxiliary surfaces inside and outside of the “Mummy” and also inside and outside of the surrounded semi open surface like the room (figure 2). Along the surfaces of the “Mummy” and so called the room, as it is possible homogeneously, we distribute the N and M numbers of points, correspondingly. On these auxiliary surfaces from both sides are distributed the same numbers combined auxiliary sources with unknown complex coefficients, which have meaning of the criterion weigh [2]. These unknown complex amplitudes of the auxiliary sources must be found by the boundary conditions satisfaction using the collocation method for the scattered field on the human body model - as on the dielectric (the continuity of the electric and magnetic field tangential components). On the semi open surface inside and outside (the tangential component of the electric field must be zero) and on the open parts (windows) of the room (as on the dielectric) – continuity of the fields.

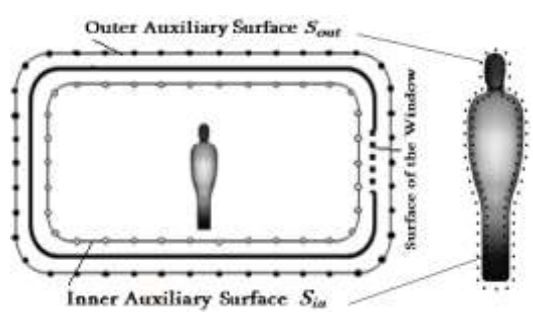

Figure 2. MAS model of cavity with using auxiliary surfaces

So, according to the proposed algorithm the open parts of window are considered as the free media with the permittivity of the air.

The combined dipole (Huygens source) was used as auxiliary source for the calculations. Its field is represented by the following expressions:

$$\vec{E}_{comb} = \vec{E}_{el} + \sqrt{\mu/\varepsilon}\vec{E}_{mag},\ \vec{H}_{comb} = \vec{H}_{el} + \sqrt{\mu/\varepsilon}\vec{H}_{mag}$$

where $\vec{E}_{el}$, $\vec{H}_{el}$ and $\vec{E}_{mag}$, $\vec{H}_{mag}$ - rather field of the electric and magnetic dipoles:

$$\vec{E}_{el} = \left(e^{ikR}/4\pi\varepsilon\right)\left\{\left(1/R^3 - ik/R^2\right)\left[3\vec{R}_0\cdot\left(\vec{R}_0\cdot\vec{p}_{el}\right) - \vec{p}_{el}\right] - \left(k^2/R\right)\left(\vec{R}_0\times\left(\vec{R}_0\times\vec{p}_{el}\right)\right)\right\},$$

$$\vec{E}_{mag} = \sqrt{\mu/\varepsilon}\left(k^2 e^{ikR}/4\pi\right)\left(1/R^2 - ik/R\right)\left(\vec{p}_{mag}\times\vec{R}_0\right),$$

$$\vec{H}_{el} = \left(i\omega e^{ikR}/4\pi\right)\left(1/R^2 - ik/R\right)\left(\vec{R}_0\times\vec{p}_{el}\right),$$

$$\vec{H}_{mag} = \left(e^{ikR}/4\pi\right)\left\{\left(1/R^3 - ik/R^2\right)\left[3\vec{R}_0\cdot\left(\vec{R}_0\cdot\vec{p}_{mag}\right) - \vec{p}_{mag}\right] - \left(k^2/R\right)\left(\vec{R}_0\times\left(\vec{R}_0\times\vec{p}_{mag}\right)\right)\right\}.$$

Here $\vec{R}_0$ is the unit vector, directed out of the dipole to the observation point, R is a distance between dipole and the observation point. $\vec{p}_{el}$ and $\vec{p}_{mag}$ are the unit polarization vectors of these dipoles. The system of the auxiliary sources, distributed on each auxiliary surface must describe the scattered field in the opposite part of the space.

Unknown field inside of the body is the sum of the inner auxiliary sources field:

$$\vec{E}^{in}_{body} = \sum_{n=1}^{N}\left(a_n\vec{E}'^{out}_{comb} + a'_n\vec{E}'^{out}_{comb}\right),\ \ \vec{H}^{in}_{body} = \sum_{n=1}^{N}\left(a_n\vec{H}'^{out}_{comb} + a'_n\vec{H}'^{out}_{comb}\right).$$

The field around the mummy and inside of the room $\vec{E}^{out}_{body}$, $\vec{H}^{out}_{body}$ is represented by the sum of the field of room's outer auxiliary sources and mummy's inner auxiliary sources.

$$\vec{E}^{out}_{body} = \sum_{n=1}^{N}\left(b_n\vec{E}^{in}_{comb} + b'_n\vec{E}'^{in}_{comb}\right) + \sum_{n=1}^{N}\left(c_n\vec{E}^{out}_{comb} + c'_n\vec{E}'^{out}_{comb}\right),$$

$$\vec{H}^{out}_{body} = \sum_{n=1}^{N}\left(b_n\vec{H}^{in}_{comb} + b'_n\vec{H}'^{in}_{comb}\right) + \sum_{n=1}^{N}\left(c_n\vec{H}^{out}_{comb} + c'_n\vec{H}'^{out}_{comb}\right),$$

The field outside of the room is the sum of base station antenna's field and room's inner auxiliary sources fields:

$$\vec{E}^{out} = \vec{E}_{inc} + \sum_{n=1}^{N}\left(d_n\vec{E}^{in}_{comb} + d'_n\vec{E}'^{in}_{comb}\right),\ \ \vec{H}^{out} = \vec{H}_{inc} + \sum_{n=1}^{N}\left(d_n\vec{H}^{in}_{comb} + d'_n\vec{H}'^{in}_{comb}\right).$$

For unknown complex coefficients a_n, a'_n, b_n, b'_n, c_m, c'_m, d_m, d'_m, where $n = 1, 2, ...N$, $m = 1, 2, ..., M$ we get the linear algebraic equation system, the number of which coincides to the number of unknowns.

3. MAS METHODOLOGY FOR MODELING VARIOUS SURFACE TRANSMISSION AND REFLACTION PROPERTIES

In this paper we introduce a new approach to use the MAS methodology to easily simulate the surface transparency variations by means of the changing the accuracy of the boundary conditions satisfaction, which is necessary to study how to influence room's walls transparency variation on the EM field exposure. In order to compute the wall transparency coefficient the effect of averaged boundary conditions is used. According to our idea the wall transparency can be regulated by changing the collocation point number on the auxiliary surface. Decreasing this number results in increase of total solution error. Simulation results show that in case with fewer collocation points the inner field can pass between these points, resulting in transparency of the surface.

For quantitative analysis of the transparency coefficient a plane wave diffraction problem on an infinite perfectly conducting surface has been considered. The surface has been substituted by a system of collocation points with some periodicity, where the satisfaction of the boundary conditions was required. The detailed analysis dependency of the R - reflection and T - transparency coefficients on the collocation point's density with N/λ^2 has been investigated and the results are shown on figure 3, 4 and 5.

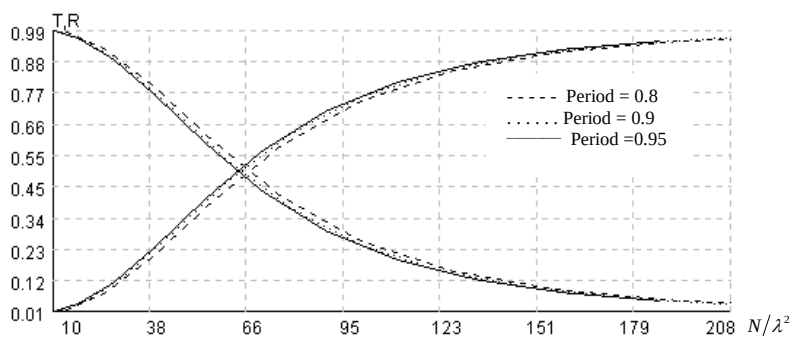

Figure 3. Transmission and Reflection coefficients dependence on the collocation points, for the different lattice period, when d=0.08

Dependencies between T - transmission and R - reflection coefficients for different mesh periods and density of the collocation points are presented on figure 3. The density of the collocation points is presented in N/λ^2 - units. The d - is the distance between the study surface and auxiliary sources. From figure 3 it can be seen that the reflection and transmission cofficients do not depend on the mesh period.

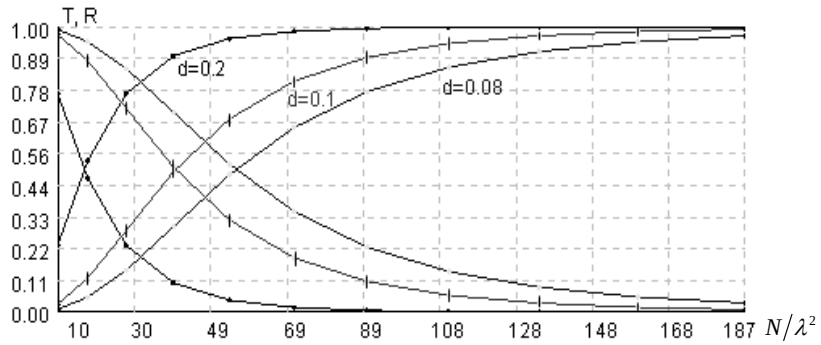

Figure 4. Transmission and reflection coefficients dependence on the collocation points, for the different *d* (distance between the collocation points and auxiliary sources).

The *T* and *R* coefficient dependency on the *d* distance is presented on figure 4. It can be seen that with the increase of the *d* distance, the *T* and *R* coefficients converge faster.

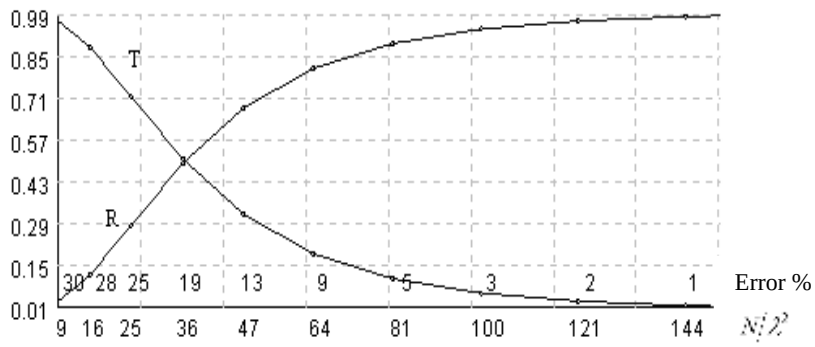

Figure 5. Transmission and reflection coefficients dependence on the collocation point's density and the calculation error, when *d*=0.1

The transmission and reflection coefficients are shown along with the error of solution (figure 5). It can be seen that with the increase of the collocation points the accuracy of boundary condition satisfaction increases and the error of the solution is decreased. At the same time the transmission coefficient decreases too, and visaversa, when the number of collocation points decreases, the transmission coeffisiets is augmented.

So, by choosing the correct density, the desired transparency coefficient *T* can be obtained, which may better correspond to a real-world scenario. Since the transparency coefficient values have been obtained in wave length units, the obtained results will be valid for all frequencies.

Our final goal is to find the near field distribution inside of the human body as well as inside and outside of the room. We have to estimate human exposure and also radiated far

field pattern. We have created a new program package based on proposed methodology and investigated several exposure scenarios.

3. RESULTS OF NUMERICAL SIMULATIONS

Several exposure scenarios with different transparency coefficients have been investigated by means of the proposed algorithm. The calculations were conducted for frequencies used in the standard mobile frequency range. The human model like Mummy (figure 2) had following dimensions: height 1.67m, shoulder width 0.46m, head diameter 0.175m. Complex permittivity, ε=45+i2, (an averaged value considering blood, muscle and bones). All calculations are carried out on a room with dimensions: 4x3x2.5 (m^3), window size is 1.4x1.1 (m^2). The EM field incidence angle is 30^0 which means, that base station antenna is located sufficiently near. Several scenarios have been studied for two different human model positions (when human is located near the window and far from the window) at 900 MHz and 1800 MHz. Obtained results are presented below. Values of the near field distribution and SAR are provided in the relative units.

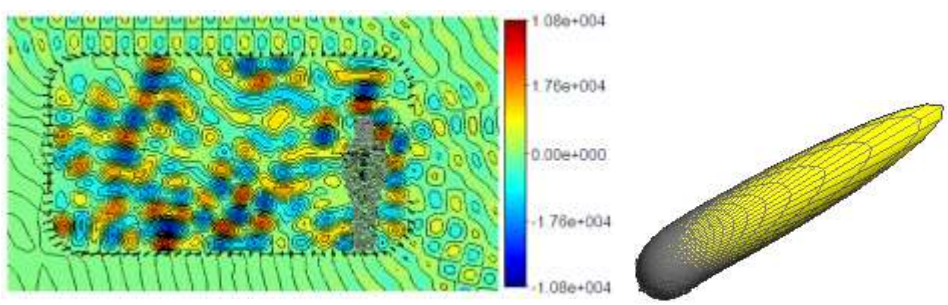

a) b)

Figure 6. Near field distribution in the room (a) and far field pattern (b) at 900 MHz, when T=0.75

Figure 6 a) shows the near field distribution in the room and nearby, when the human model is located near the window. Figure 6 b) represents reradiated far field pattern, which is directed to the base station's position. Ruler on the figure shows the maximal value of the field located near the Mummy's head. Room walls are transparent and the value of the transparency equals to the 0.75. Figure 7 a) shows the point SAR distribution. The maximal value is 1.3 W/Kg. Figure 7 b) represents the frequency characteristic of the room with Mummy. As we see because of the high transparency of the room walls, the resonance effects are minimal without resonant frequency discrimination.

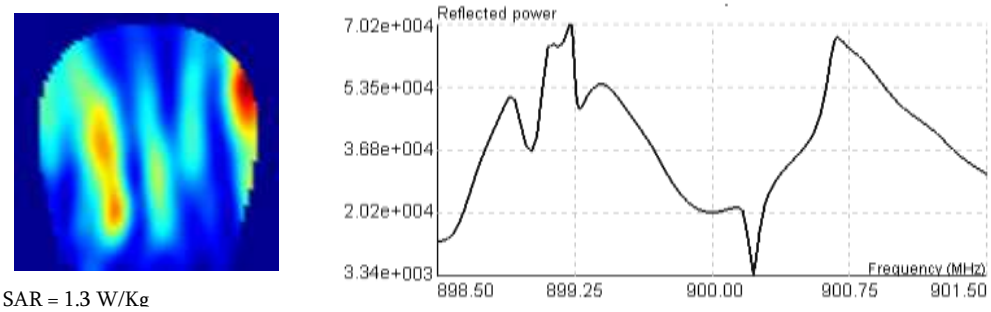

SAR = 1.3 W/Kg

a) b)

Figure 7. SAR distribution inside of human head (a) and frequency characteristic (b) for the room. The frequency is 900 MHz, human model is located near the window and *T*=0.75

The figures 8 and 9 show the results of similar study for the room with low transparency T=0.22. As it is expected the near field and SAR values are almost 10 times higher, because of the high Q factor of the room, as a resonator.

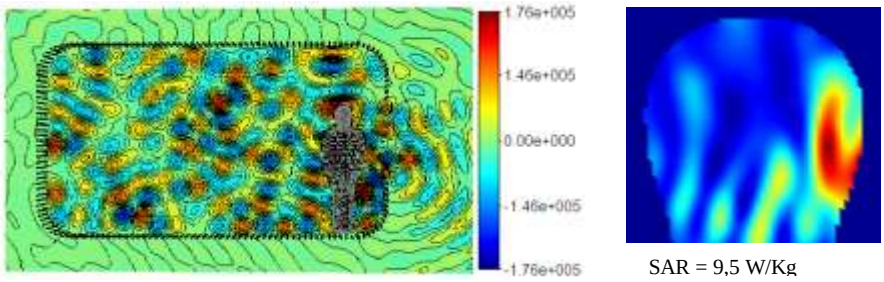

SAR = 9,5 W/Kg

a) b)

Figure 8. (a) Near field distribution in the room and (b) SAR distribution inside of the human head at 900 MHz, when human model is located near the window. *T*=0.22

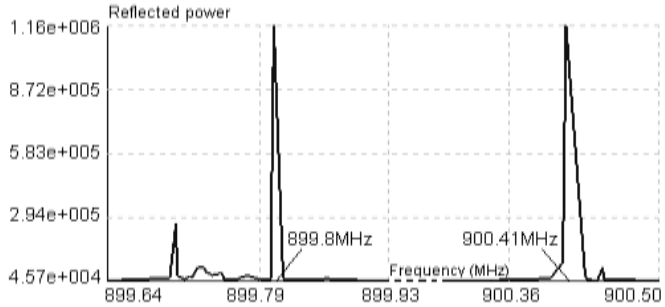

Figure 9. Frequency characteristic for the room at 900 MHz, when human model is located near the window, when *T*=0.22

Figure 9 shows the detailed frequency characteristic on which we see two sharp, discriminated resonance frequencies 899.8MHz and 900.41MHz. Figure 10 corresponds to the first resonant case. We can see that maximal field value in this case is one orders higher.

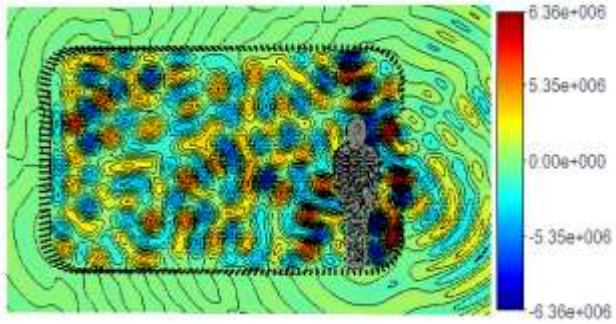

Figure 10. Near field distribution in the room at 899.79 MHz resonant frequency, when human model is located near the window and *T*=0.22

The next results show the situation, when the human is located far and opposite from the window, near the wall. The near field and SAR values in this case are higher (figure 11), because more energy goes inside of the room, than in the previous cases when human was located near the window.

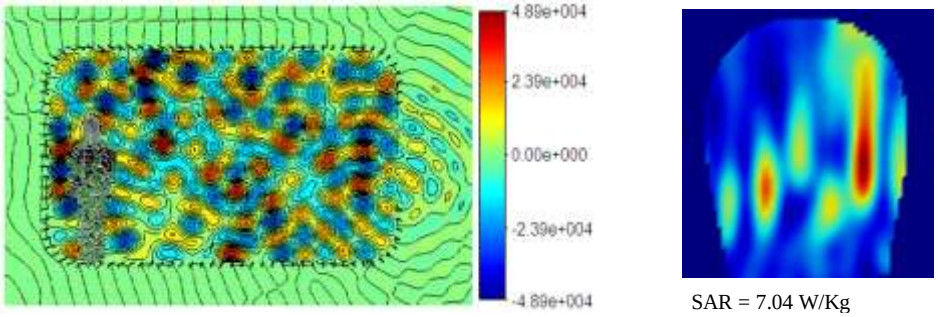

a) b)

Figure 11. (a) Near field distribution in the room and (b) SAR distribution inside of human head at 900 MHz, when human model is located far from the window and *T*=0.75

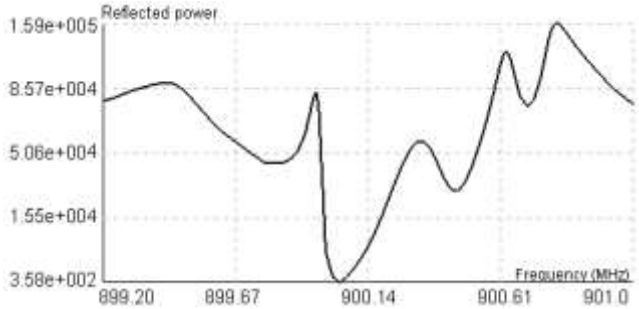

Figure 12. Frequency characteristic for the room at 900 MHz, when human model is located far from the window, when *T*=0.75

The frequency characteristic has not discriminated resonances in that case too because of the high transparency T=0.75 (figure 12). Figure 13 shows the case of the low value of

transparency (T=0.22) when the resonant effect increases. Maximal near field and SAR values are higher than it was when the human was near the window (figure 8).

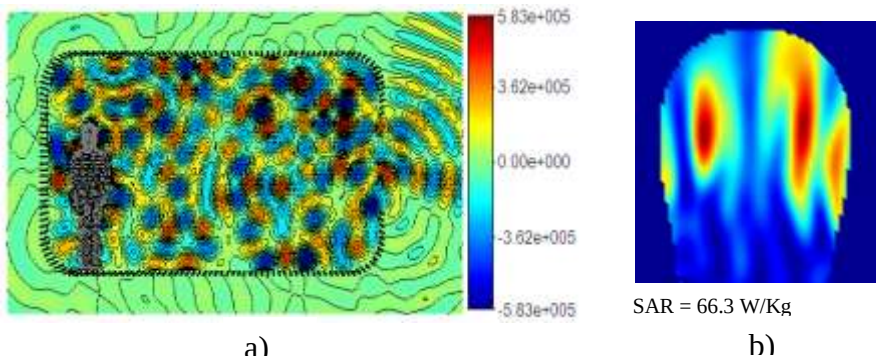

Figure 13. (a) Near field distribution in the room and (b) SAR distribution inside of human head at 900 MHz, when human model is located far from the window and *T*=0.22

In this case, the frequency characteristic has sharp resonance (figure 14) and at that resonance, the near field distribution is presented on the figure 15.

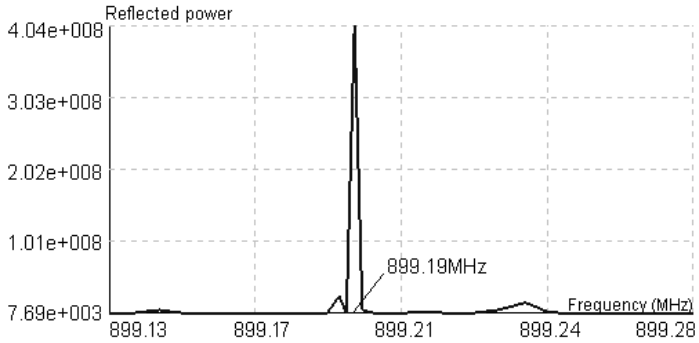

Figure 14. Frequency characteristic for the room at 900 MHz, when human model is located far from the window, when *T*=0.22

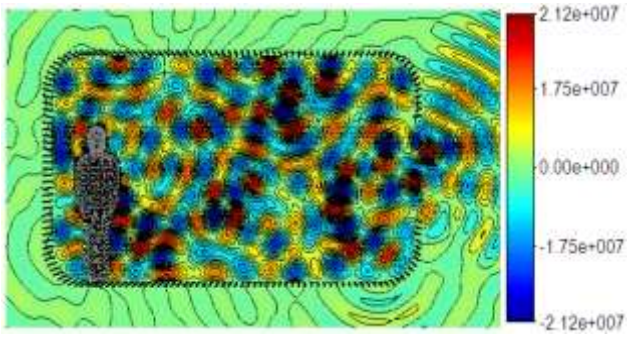

Figure 15. Near field distribution in the room at 899.19 MHz resonant frequency, when human model is located near the window and T=0.22

We see clearly that, because of the small transparency we have multiple reflections of the inner field and energy storage inside the room, the resonant field amplitude is almost 10 times higher than in case when the human was near the window.

Next are presented investigation for higher frequency 1800 MHz, which also corresponds to the main frequency of the mobile phone. We have considered two cases, for different position of the human. There are provided corresponding near field distributions (figure 16, 17).

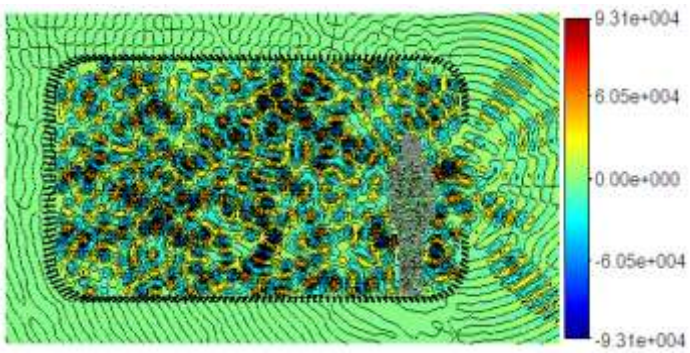

Figure 16. Near field distribution in the room at 1800 MHz, when human model is located near window; T=0.75

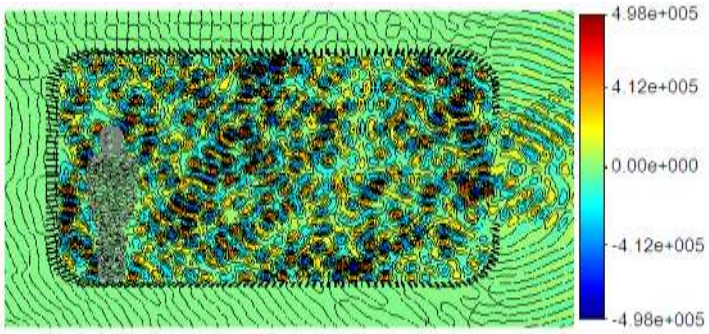

Figure 17. Near field distribution in the room at 1800 MHz, when human model is located far window; T=0.75

Because of the high losses at this frequency the depth of the field penetration in the human model is smaller than for the lower frequencies. The most part of the radiated energy goes through the window.

If we compare figure 16 and 17 we can see that when the human is located near the wall, far from the window, the high field values field inside of the room are bigger.

The parameters of the computer used to solve this problem are the next: Dual Intel Xeon x5650 with the 24 threads and 64Gb of RAM.

4. CONCLUSION

The base station antenna's field diffraction on the room with the homogeneous human model inside is studied. The new, MAS based, program package has been used for simulations. The MAS methodology was used to simulate surface with different transparency. Numerical experiments provided by this program package showed that the field, radiated by the base station antenna, could be amplified at some resonant frequencies inside of the room. The reason of this is that at the considered frequencies room acts as the resonator. So in order to estimate the maximal allowed value of the field, the resonator properties of the room must be taken into account. The position of the human inside of the room changes significantly the near field distribution inside of the room. In contrast to the FDTD, the MAS give us the possibility to study the near fields around the human model considering the walls and windows. It also makes possible to examine the resonance phenomena and control the accuracy of the solution. A big attention is paid to the transparency of the walls, which is strictly related to the accuracy of the solution and to the number of the collocation points. The calculations, conducted with the created program package, showed the presence of resonance and reactive fields in several big scenarios which could be dangerous for a human.

ACKNOWLEDGMENT

This study is supported by Shota Rustaveli National Science Foundation grant #30/09.

REFERENCES

[1] V. Jeladze, I. Petoev, V. Tabatadze, M. Prishvin, R. Zaridze, "The Method of Auxiliary Sources for Study of Resonant Field Effects upon a Human Models for Big Scenarios", Journal of Communications Technology and Electronics, Moscow, Russia. Accepted for publication on 2015.

[2] V. Jeladze, M. Prishvin, R. Zaridze, "RF Exposure Simulation using Considering Blood Perfusion for a Child and Woman Models", Journal of Applied Electromagnetism (JAE), 2014, Vol. 16, No.2, pp. 26-23

[3] D. Kakulia, K. Tavzarashvili, V. Tabatadze, R. Zaridze, "Investigation of the field distribution inside the rooms located near the base stations antenna". Proceedings of

VIII-th International Seminar/Workshop on Direct and Inverse Problems of Electromagnetic and Acoustic Wave Theory (DIPED-2003), Lviv, September 23-25, 2003. pp. 162-165.

[4] R. Zaridze, G. Bit-Babik, K. Tavzarashvili, N. Uzunoglu, D. Economou. "Wave Field Singularity Aspects Large-Size Scatterers and Inverse Problems," IEEE Transactions on Antennas and Propagation, vol. 50, No. 1, January 2002, pp. 50 - 58.

[5] Petoev I., Tabatadze V., Kakulia D., Zaridze R., “Application of the Method of Auxiliary Sources to the Electromagnetic Field’s Diffraction on the Some Metal-dielectric Structures”, Journal of Communications Technology & Electronics, 2013, Vol. 58, No 5, pp. 404-416

APPLICATION OF LIMIT RELATIONS METHOD TO THOMSON'S MODEL OF HIGH-FREQUENCY INDUCTIVE DISCHARGE OF FINITE LENTH

A.P. Kirpichnikov
Kazan National Research Technological University, Kazan, Russia
e-mail : kirpichnikov@kstu.ru

Abstract

The exhaustive analytical solution to the task about the structure of quasistationary electromagnetic field of high-frequency inductive discharge of finite length near the axis of plasma bunch is given.

1. INTRODUCTION

In the series of works [1-5] on the basis of the idea of the limit relations for high-frequency inductive (HFI) discharge, the structure of quasistationary electromagnetic field of high-frequency inductive discharge of finite length near the axis of plasma bunch has been analyzed. In these works there has been offered a new method of approximate integration of differential equation system with partial derivatives, allowing to describe unambiguously the structure of these equations solutions in the neighborhood of points in which expressions for secondary characteristics of the process described by the equations (i.e. these combinations of unknown quantities entering input equations) contain indeterminacies of $0/0$ type.

The equations of electromagnetic field of HFI discharge in works [1-5] were recorded in physical variables amplitude-phase. Meanwhile, there is one more analytical model of HFI discharge constructed in the approximation that conduction in the discharge $\sigma(r,z)$ is considered equal to some constant value in the whole plasmoid volume (and not just in its near-axial zone as it considered in [1-5]). It is clear, that in the limit $r\to 0$ both models have to give close results.

The model of constant conductivity which is also possible to call the canal model of HFI discharge, was essentially completed by J. Thomson in 1926 and published a year later in his well-known paper [6]. Thomson himself, as it is known, considered

unidimensional theory variant, the solution in a general case or Thomson's generalized model of HFI discharge in the two-dimensional statement of the problem is presented in the paper [7].

In this work the method of limit relations is applied immediately to Thomson's model equations, after that the obtained result is compared with known exact solutions for amplitudes and phase characteristics of all components of electromagnetic field in the discharge.

2. THE SOLUTION OF THE PROBLEM IN ONE-DIMENSIONAL APPROXIMATION

Let us consider a one-dimensional case as the first stage of the task. The equation system of Thomson's one-dimensional model takes the form [6, 7]

$$\frac{\partial E_\varphi}{\partial r} + \frac{E_\varphi}{r} = -i\frac{\omega}{c}H_z;$$

$$\frac{\partial H_z}{\partial r} = -\frac{4\pi}{c}\sigma E_\varphi,$$

whence the limit relations result

$$\left.\frac{\partial E_\varphi}{\partial r}\right|_{r=0} = -i\frac{\omega}{2c}H_z(0) \quad \text{и} \quad \sigma(r=0) = -\frac{c}{4\pi}\frac{\left.\frac{\partial H_z}{\partial r}\right|_{r=0}}{E_\varphi(0)}.$$

In these relations E_φ and H_z – complex amplitudes of electric and magnetic fields, ω - an oscillation frequency of the HF field, c – light speed in vacuum (in Gaussian system of units). Due to the symmetry on the axis of HFI discharge the azimuthal electric field is equal to zero, but $\sigma(r=0) \neq 0$, so according to l'Hôpital's rule,

$$\sigma(r=0) = -\frac{c}{4\pi}\frac{\left.\frac{\partial^2 H_z}{\partial r^2}\right|_{r=0}}{\left.\frac{\partial E_\varphi}{\partial r}\right|_{r=0}} = \frac{c^2}{2\omega\pi i}\frac{\left.\frac{\partial^2 H_z}{\partial r^2}\right|_{r=0}}{H_z(0)}$$

(the second limit relation), so, near the plasmoid axis

$$H_z(r) = H_z(0)\left[1 + i\frac{\pi\omega\sigma(0)}{c^2}r^2\right] \tag{1}$$

or

$$\overline{H}_z(r) + i\overline{H}_z(r) = \left[\overline{H}_z(0) + i\overline{H}_z(0)\right]\left[1 + i\frac{\pi\omega\sigma(0)}{c^2}r^2\right] =$$

$$= \overline{H}_z(0) - \frac{\pi\omega\sigma(0)}{c^2}\overline{\overline{H}}_z(0)r^2 + i\left[\overline{\overline{H}}_z(0) + \frac{\pi\omega\sigma(0)}{c^2}\overline{H}_z(0)r^2\right].$$

where values with one and two over-lines mean the real and imaginary parts of corresponding complex value.

Further, according to physically trivial boundary conditions we will suppose $\overline{H}_z(0) = 0$, $\overline{\overline{H}}_z(0) = H_z^a(0)$, and then

$$H_z^a(r) = \sqrt{\overline{H}_z^2 + \overline{\overline{H}}_z^2} = H_z^a(0)\sqrt{1 + \frac{\pi^2\omega^2\sigma^2(0)}{c^4}r^4} \approx$$

$$\approx H_z^a(0)\left[1 + \frac{\pi^2\omega^2\sigma^2(0)}{2c^4}r^4\right]; \tag{2}$$

$$\varphi_{H_z}(r) = arctg\frac{\overline{\overline{H}}_z}{\overline{H}_z} = arctg\left[-\frac{1}{\frac{\pi\omega\sigma(0)}{c^2}r^2}\right] \approx \frac{\pi}{2} + \frac{\pi\omega\sigma(0)}{c^2}r^2. \tag{3}$$

It is easy to see that in this case

$$\frac{1}{r}\frac{\partial}{\partial r}\left(rE_\varphi\right) = -i\frac{\omega H_z(0)}{c}\left[1 + i\frac{\pi\omega\sigma(0)}{c^2}r^2\right]$$

(the formula of the second approximation), from which

$$E_{\varphi}(r) = -i\,\frac{\omega\, H_z(0)}{2c}\; r\left[1 + i\,\frac{\pi\omega\sigma(0)}{2c^2}\,r^2\right] = \frac{\omega\, H_z^a(0)}{2c}\; r\left[1 + i\,\frac{\pi\omega\sigma(0)}{2c^2}\,r^2\right],$$

therefore

$$E_{\varphi}^a(r) \approx \frac{\omega H_z^a(0)}{2c}\,r \tag{4}$$

and

$$\varphi_{E_{\varphi}}(r) = arctg\,\frac{\overline{\overline{E}}_{\varphi}}{\overline{E}_{\varphi}} = arctg\left[\frac{\pi\omega\sigma(0)}{2c^2}\,r^2\right] \approx \frac{\pi\omega\sigma(0)}{2c^2}\,r^2. \tag{5}$$

The corresponding solutions for equations recorded in physical variables, obtained in works [3-5], take the form

$$H_z^a(r) \approx H_z^a(0)\left[1 + \frac{\omega^2\pi^2\sigma^2(0)}{4c^4}\,r^4\right]; \tag{6}$$

$$\varphi_{H_z}(r) \approx \frac{\pi}{2} + \frac{\omega\,\pi\,\sigma(0)}{c^2}\,r^2; \quad E_{\varphi}^a \approx \frac{\omega H_z^a(0)}{2c}\,r; \quad \varphi_{E_{\varphi}}(r) \approx \frac{\omega\,\pi\,\sigma(0)}{2c^2}\,r^2.$$

As we see, the method of the limit relations in Thomson's one-dimensional problem gives the true result for three values $\varphi_{H_z}(r)$, $E_{\varphi}^a(r)$ and $\varphi_{E_{\varphi}}(r)$ out of four, but contains difference in formula (2) for $H_z^a(r)$, where the coefficient at r^4 is twice higher in comparison with the earlier found dependence (6).

It is clear, that this error is connected here with the neglect of decomposition (1) of summands, containing the highest (in this case the fourth) exponential degree of smallness according to *r*, that, in turn, is the peculiarity of limit relations method application in the complex problem statement. To receive the true result, in this case it is necessary to resort to the usage of the second approximation within which, as it is easy to see, we obtain

$$H_z(r) = H_z(0) - \frac{4\pi\sigma(0)}{c}\int_0^r E_\varphi(r)\,dr = H_z(0)\left[1 + i\frac{\pi\omega\sigma(0)}{c^2}r^2 - \frac{\pi^2\omega^2\sigma^2(0)}{4c^4}r^4\right]$$

and then

$$H_z^a(r) = H_z^a(0)\sqrt{1 + \frac{\pi^2\omega^2\sigma^2(0)}{c^4}r^4 - \frac{\pi^2\omega^2\sigma^2(0)}{2c^4}r^4} \approx$$

$$\approx H_z^a(0)\left[1 + \frac{\pi^2\omega^2\sigma^2(0)}{4c^4}r^4\right]$$

in accordance with the formula (6).

3. THE SOLUTION IN TWO-DIMENSIONAL FORMULATION OF THE PROBLEM

Let us pass to a two-dimensional problem statement. The two-dimensional analog of equations of an electromagnetic field of HFI discharge takes the form [7]

$$\frac{1}{r}\frac{\partial}{\partial r}(rE_\varphi) = -\frac{i\omega}{c}H_z; \tag{7}$$

$$\frac{\partial H_z}{\partial r} - \frac{\partial H_r}{\partial z} = -\frac{4\pi}{c}\sigma E_\varphi; \tag{8}$$

$$\frac{1}{r}\frac{\partial}{\partial r}(rH_r) + \frac{\partial H_z}{\partial z} = 0; \tag{9}$$

$$\frac{\partial E_\varphi}{\partial z} = \frac{i\omega}{c}H_r, \tag{10}$$

where H_r is the complex amplitude of radial magnetic field in the discharge. Hence the limit relations

$$\sigma(r=0)=-\frac{c}{4\pi}\frac{\left.\frac{\partial H_z}{\partial r}\right|_{r=0}-\left.\frac{\partial H_r}{\partial z}\right|_{r=0}}{E_\varphi(0)} \tag{11}$$

and

$$\sigma(r=0)=-\frac{c}{4\pi}\frac{\left.\frac{\partial^2 H_z}{\partial r^2}\right|_{r=0}-\left.\frac{\partial^2 H_r}{\partial z\,\partial r}\right|_{r=0}}{\left.\frac{\partial E_\varphi}{\partial r}\right|_{r=0}}=\frac{c^2}{2\omega\pi i}\frac{\left.\frac{\partial^2 H_z}{\partial r^2}\right|_{r=0}-\left.\frac{\partial^2 H_r}{\partial z\,\partial r}\right|_{r=0}}{H_z(0,z)}\,. \tag{12}$$

From formulas (11), (12) it follows that at small values of the amplitude radial coordinate r the longitudinal and radial components of magnetic field submit to the system of equations

$$\frac{\partial H_z}{\partial r}-\frac{\partial H_r}{\partial z}=i\frac{2\pi\omega\sigma(0,z)}{c^2}H_z(0,z)\,r\,; \tag{13}$$

$$\frac{1}{r}\frac{\partial}{\partial r}(rH_r)+\frac{\partial H_z}{\partial z}=0\,. \tag{14}$$

The first equation in this system is evidently the first nonzero summand of the function decomposition $F=\frac{\partial H_z}{\partial r}-\frac{\partial H_r}{\partial z}$ into its Maclaurin series. Now let us differentiate the equation (13) on r, and the equation (14) on z. Then we will obtain

$$\frac{\partial}{\partial r}\left(r\frac{\partial H_z}{\partial r}\right)-\frac{\partial}{\partial z\partial r}(rH_r)=i\frac{4\pi\omega\sigma(0,z)}{c^2}H_z(0,z)\,;$$

$$\frac{\partial}{\partial z\partial r}(rH_r)+r\frac{\partial^2 H_z}{\partial z^2}=0\,.$$

Combining these two expressions, we will find the linear differential equation with partial derivatives for the amplitude of longitudinal component of a magnetic field $H_z(r,z)$ near the plasmoid axis

$$\frac{\partial^2 H_z}{\partial r^2}+\frac{1}{r}\frac{\partial H_r}{\partial r}+\frac{\partial^2 H_z}{\partial z^2}=i\frac{4\pi\omega\sigma(0,z)}{c^2}H_z(0,z)\,. \tag{15}$$

Next let us put approximately the value of conduction $\sigma(0,z)$ as equal to its some average along the plasmoid length to the value $\sigma(0,z)\approx\sigma_{cp}=const$. It is possible to show accurately [8, 9] that due to the slowness of the parameter $4\pi\omega/c^2$ in the right member of the equation (15), the solution of the equation, modified in such a way, with the rise of variable z will strive asymptotically for the solution of the input equation. From the point of view of physics, this assumption obviously corresponds to the usage of some kind of a canal model for the high-frequency inductive discharge.

The equation (11) with the condition $\sigma(0,z)\approx\sigma_{cp}=const$ taken into account has the exact solution which can be received by means of Fourier method of variables separation by representation of the required function $H_z(r,z)$ in the form of the product of functions $H_z(r,z)=H_1(r)H_2(z)$ in all definition range of the function $H_z(r,z)$. In this case the equation (15) will be written down as

$$H_2\frac{\partial^2 H_1}{\partial r^2}+\frac{H_2}{r}\frac{\partial H_1}{\partial r}+H_1\frac{\partial^2 H_2}{\partial z^2}=i\frac{4\pi\omega\sigma_{cp}}{c^2}H_1(0)H_2(z)\,. \tag{16}$$

Having divided the relation (16) into the product $H_1(r)H_2(z)$, we will find

$$\frac{1}{H_1}\frac{\partial^2 H_1}{\partial r^2}+\frac{1}{rH_1}\frac{\partial H_1}{\partial r}+\frac{1}{H_2}\frac{\partial^2 H_2}{\partial z^2}=i\frac{4\pi\omega\sigma_{cp}}{c^2}\frac{H_1(0)}{H_1}\,.$$

The last equation, as it is easy to see, is split into the system of two differential equations for unknown functions $H_1(r)$ and $H_2(z)$

$$\frac{\partial^2 H_1}{\partial r^2}+\frac{1}{r}\frac{\partial H_1}{\partial r}-C\,H_1=i\frac{4\pi\omega\sigma_{cp}}{c^2}H_1(0)\,; \tag{17}$$

$$\frac{\partial^2 H_2}{\partial z^2}+CH_2=0\,, \tag{18}$$

in which C – some constant of splitting (positive number), the precise meaning of which has to be defined on the basis of boundary conditions.

The problem of the equation (15) solution is reduced in this case, firstly, to the solution of Cauchy problem relating to the radial coordinate r for function $H_1(r)$, and, secondly, to the solution of the boundary value problem relating to the longitudinal coordinate z for function $H_2(z)$.

The solution of the second equations of the system (17)-(18) is obvious:

$$H_2(z) = A Sin\left(\sqrt{C}\, z\right) + B Cos\left(\sqrt{C}\, z\right).$$

In the subspace of the central section of the plasmoid at z=0 there should be satisfied conditions

$$H_r(z=0)=0\,; \quad \left.\frac{\partial H_z}{\partial z}\right|_{z=0} = 0\,,$$

whence it follows that in this case the value of the constant value A is equal to zero, therefore we have

$$H_2(z) = H_2(0) Cos\left(\sqrt{C} z\right). \tag{19}$$

In its turn, written down in this way, the equation (17), is, as it is easy to see, one of the alternatives of Bessel inhomogeneous equation

$$\frac{\partial^2 y}{\partial x^2} + \frac{1}{x}\frac{y}{\partial x} - C\, y = a\, x^{2n}$$

for an unknown function y. Its general solution for the right member representing an even degree of the argument, is given in work [10]:

$$y(x) = y(0)\, I_0(\sqrt{C}\, x) + \frac{\left(2^n\, n!\right)^2 a}{C^{n+1}} \left[I_0(\sqrt{C}\, x) - \sum_{p=0}^{n} C^p \left(\frac{x^p}{2^p\, p!} \right)^2 \right],$$

where I_0 - Bessel modified function of the zero order. Hence, we have

$$H_1(r)=H_1(0)\left\{I_0(br)+i\frac{4\pi\,\omega\,\sigma_{cp}}{b^2\,c^2}\,\left[I_0(br)-1\right]\right\},$$

that is

$$H_z(r,z)=H_z(0,0)\left\{I_0(br)+i\frac{4\pi\,\omega\,\sigma_{cp}}{b^2\,c^2}\,\left[I_0(br)-1\right]\right\}Cos(bz)\,, \tag{20}$$

where $b=\sqrt{C}=\frac{1}{L}arcCos\left[\frac{H_z(0,\mathrm{L})}{H_z(0,0)}\right]$, L – the plasmoid length. According to boundary conditions $\overline{H}_z(0,0)=0$, $\overline{\overline{H}}_z(0,0)=H_z^a(0,0)$, and then

$$\overline{\overline{H}}_z(r,z)=H_z^a(0,0)\,I_0(br)\,Cos(bz)\,;$$

$$\overline{H}_z(r,z)=-\frac{4\pi\,\omega\,\sigma_{cp}}{b^2\,c^2}\,H_z^a(0,0)\left[I_0(br)-1\right]Cos(bz)\,,$$

from where

$$H_z^a(r,z)=H_z^a(0,0)\sqrt{I_0^2(br)+\frac{16\pi^2\omega^2\sigma_{cp}^2}{b^4c^4}\left[I_0(br)-1\right]^2}\;Cos(bz)\approx$$

$$\approx H_z^a(0,0)\,I_0(br)\left\{1+\frac{8\pi^2\omega^2\sigma_{cp}^2}{b^4c^4}\left[\frac{I_0(br)-1}{I_0(br)}\right]^2\right\}Cos(bz)\,; \tag{21}$$

$$\varphi_{H_z}(r,z)=arctg\left\{-\frac{I_0(br)}{\frac{4\pi\omega\sigma_{cp}}{b^2c^2}\left[I_0(br)-1\right]}\right\}\approx\frac{\pi}{2}+\frac{4\pi\omega\sigma_{cp}}{b^2c^2}\,\frac{I_0(br)-1}{I_0(br)}\,. \tag{22}$$

The equations (7) and (9) give then the following expressions for complex amplitudes of radial magnetic and azimuthal electric fields in the discharge:

$$H_r(r,z)=H_z(0,0)\left\{I_1(br)+i\frac{4\pi\,\omega\,\sigma_{cp}}{b^2\,c^2}\,\left[I_1(br)-\frac{br}{2}\right]\right\}Sin(bz)=$$

$$=H_z^a(0,0)\left\{i\,I_1(br)-\frac{4\pi\,\omega\,\sigma_{cp}}{b^2\,c^2}\,\left[I_1(br)-\frac{br}{2}\right]\right\}Sin(bz)\,; \tag{23}$$

$$E_{\varphi}(r,z)=\frac{\omega H_z(0,0)}{b\,c}\left\{-i\,I_1(br)+\frac{4\pi\,\omega\,\sigma_{cp}}{b^2\,c^2}\left[I_1(br)-\frac{br}{2}\right]\right\}Cos(bz)=$$

$$=\frac{\omega H_z^a(0,0)}{b\,c}\left\{I_1(br)+i\,\frac{4\pi\,\omega\,\sigma_{cp}}{b^2\,c^2}\left[I_1(br)-\frac{br}{2}\right]\right\}Cos(bz)\,. \tag{24}$$

In these relations I_1 - Bessel modified function of the first order. In physical variables amplitude-phase we have

$$H_r^a(r,z)=H_z^a(0,0)\sqrt{I_1^2(br)+\frac{16\pi^2\,\omega^2\,\sigma_{cp}^2}{b^4\,c^4}\left[I_1(br)-\frac{br}{2}\right]^2}\;Sin(bz)\approx$$

$$\approx H_z^a(0,0)\,I_1(br)\left\{1+\frac{8\pi^2\,\omega^2\,\sigma_{cp}^2}{b^4\,c^4}\left[\frac{I_1(br)-\frac{br}{2}}{I_1(br)}\right]^2\right\}Sin(bz); \tag{25}$$

$$\varphi_{H_r}(r,z)=arctg\left[-\frac{b^2c^2}{4\pi\omega\sigma_{cp}^2}\frac{I_1(br)}{I_1(br)-\frac{br}{2}}\right]\approx\frac{\pi}{2}+\frac{4\pi\omega\sigma_{cp}^2}{b^2c^2}\frac{I_1(br)-\frac{br}{2}}{I_1(br)}\,; \tag{26}$$

$$E_{\varphi}^a(r,z)=\frac{\omega H_z^a(0,0)}{b\,c}\sqrt{I_1^2(br)+\frac{16\pi^2\,\omega^2\,\sigma_{cp}^2}{b^4\,c^4}\left[I_1(br)-\frac{br}{2}\right]^2}\;Cos(bz)\approx$$

$$\approx\frac{\omega H_z^a(0,0)}{b\,c}\,I_1(br)\left\{1+\frac{8\pi^2\,\omega^2\,\sigma_{cp}^2}{b^4\,c^4}\left[\frac{I_1(br)-\frac{br}{2}}{I_1(br)}\right]^2\right\}Cos(bz); \tag{27}$$

$$\varphi_{E_{\varphi}}(r,z)=arctg\left[\frac{4\pi\omega\sigma_{cp}^2}{b^2c^2}\frac{I_1(br)-\frac{br}{2}}{I_1(br)}\right]\approx\frac{4\pi\omega\sigma_{cp}^2}{b^2c^2}\frac{I_1(br)-\frac{br}{2}}{I_1(br)}\,. \tag{28}$$

Within the limit $b\to 0$, the obtained expressions for $H_z(r,z)$ and $E_{\varphi}(r,z)$ pass to their corresponding relations (2), (3), (4) and (5) of the one-dimensional model. As we see, the solution (20) represents a formula of the first approximation for $H_z(r,z)$, the

application of which gives, in the same way as in the one-dimensional model, an error at amplitude values determination of longitudinal component of magnetic field in the discharge. Following the procedure, presented above, i.e. substituting relations (23), (24) into the equation (7) for the complex amplitude $H_z(r,z)$, we will obtain from here the formula of the second approximation

$$H_z(r,z)=H_z(0,z)-\frac{4\pi\sigma_{cp}}{c}\int_0^r E_\varphi(r,z)\,dr+\int_0^r \frac{\partial H_r(r,z)}{\partial z}dr\approx$$

$$\approx H_z(0,0)\left\{I_0(br)+i\frac{4\pi\,\omega\sigma_{cp}}{b^2c^2}\left[I_0(br)-1\right]-\right.$$

$$\left.-\frac{16\pi^2\,\omega^2\,\sigma_{cp}^2}{b^4c^4}\left[I_0(br)-1-\frac{b^2r^2}{4}\right]\right\}Cos(bz)$$

and then

$$H_z^a(r,z)=H_z^a(0,0)Cos(bz)\times$$

$$\times\sqrt{I_0^2(br)+\frac{16\pi^2\omega^2\sigma_{cp}^2}{b^4c^4}\left[I_0(br)-1\right]^2-\frac{32\pi^2\,\omega^2\,\sigma_{cp}^2}{b^4c^4}I_0(br)\left[I_0(br)-1-\frac{b^2r^2}{4}\right]}\approx$$

$$\approx H_z^a(0,0)\,I_0(br)\times \tag{29}$$

$$\times\left\{1+\frac{8\pi^2\omega^2\sigma_{cp}^2}{b^4c^4}\left[\frac{I_0(br)-1}{I_0(br)}\right]^2-\frac{16\pi^2\omega^2\sigma_{cp}^2}{b^4c^4}\frac{I_0(br)-1-\frac{b^2r^2}{4}}{I_0(br)}\right\}Cos(bz)$$

in accordance with the relations of the one-dimensional model. For the comparison we will give the formulae, obtained in works [3-5] by the application of the limit relations method immediately to the equations, written down in amplitude-phase physical variables:

$$H_z(\mathrm{r},\mathrm{z})\approx H_z(0,0)\left\{I_0(\mathrm{br})+\frac{16\pi^2\,\omega^2\,\sigma_{cp}^2}{b^4c^4}\left[I_0(br)-1-\frac{b^2r^2}{4}\right]\right\}Cos(bz) \tag{30}$$

$$H_r(\mathrm{r,z}) \approx H_z(0,0)\left\{ I_1(\mathrm{br}) + \frac{16\pi^2\,\omega^2\,\sigma_{cp}^2}{b^4c^4}\left[I_1(br) - \frac{br}{2} - \frac{b^3r^3}{16} \right]\right\} Sin(bz), \tag{31}$$

$$E_\varphi(r,z) \approx \frac{\omega H_z(0,0)}{bc}\left\{ I_1(\mathrm{br}) + \frac{16\pi^2\,\omega^2\,\sigma_{cp}^2}{b^4c^4}\left[I_1(br) - \frac{br}{2} - \frac{b^3r^3}{16} \right]\right\} Cos(bz); \tag{32}$$

$$\varphi_{H_z}(r,z) \approx \frac{\pi}{2} + \frac{\omega\pi\sigma_{cp}}{c^2} r^2;\ \varphi_{H_r}(r,z) \approx \frac{\pi}{2} + \frac{\omega\pi\sigma_{ch}}{2c^2} r^2,\ \varphi_{E_\varphi}(r,z) \approx \frac{\omega\pi\sigma_{cp}}{2c^2} r^2. \tag{33}$$

4. DISCUSSION AND CONCLUSION

Function graphs $H_z^a(r,z), H_r^a(r,z), E_\varphi^a(r,z), \varphi_{H_z}(r,z), \varphi_{H_r}(r,z)$ and $\varphi_{E_\varphi}(r,z)$ are given in Figs. 1-6, for the transverse section $z=4$ cm of the plasmoid in the downward flow direction, they are built according to the obtained here solutions (22), (25)-(29) and relations (30)-(33) taken from works [3-4] as well.

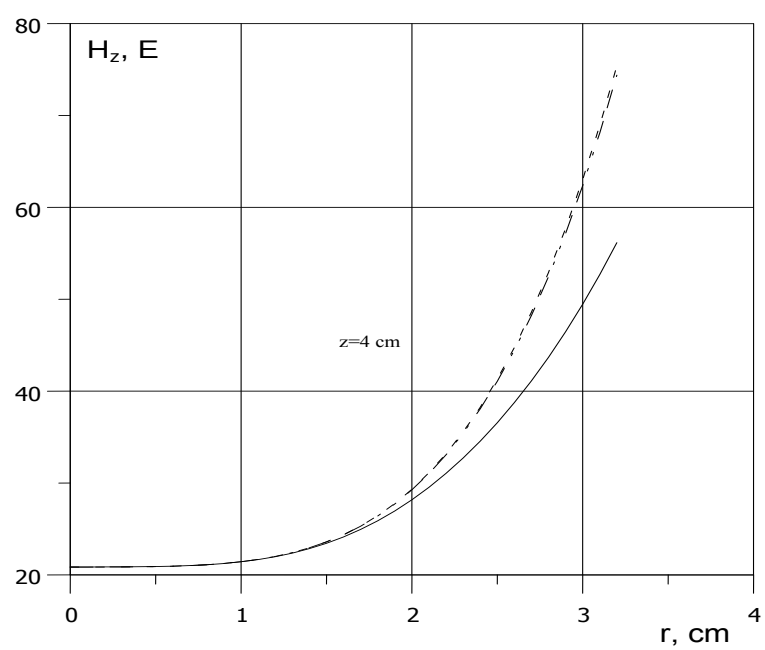

Figure 1. Amplitude of longitudinal component of magnetic field inside the plasmoid for z=4cm (the block curve – Thomson's model, dashed-line curve –method of limit relations, pecked line - method of limit relations applied to Thomson's model)

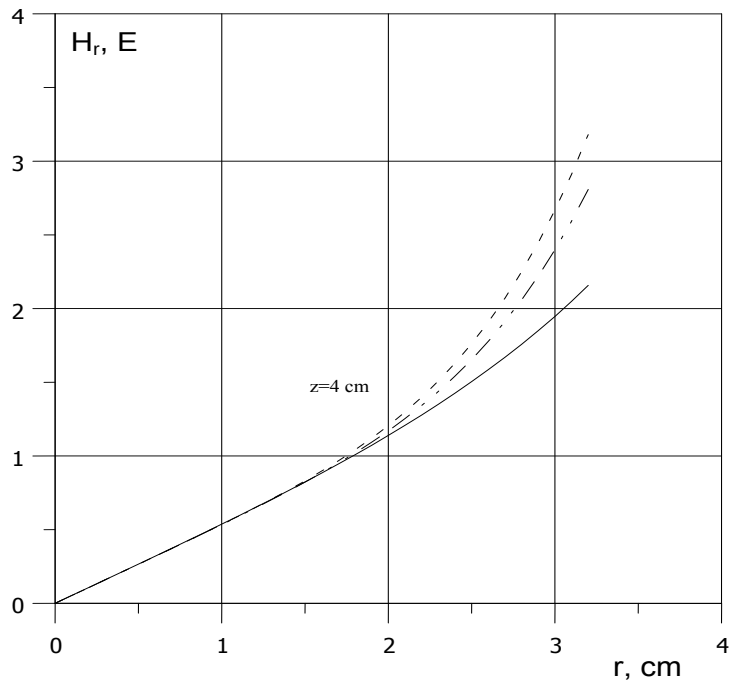

Figure 2. Amplitude of radial component of magnetic field inside the plasmoid for z=4cm (the block curve – Thomson's model, dashed-line curve – method of limit relations, pecked line - method of limit relations applied to Thomson

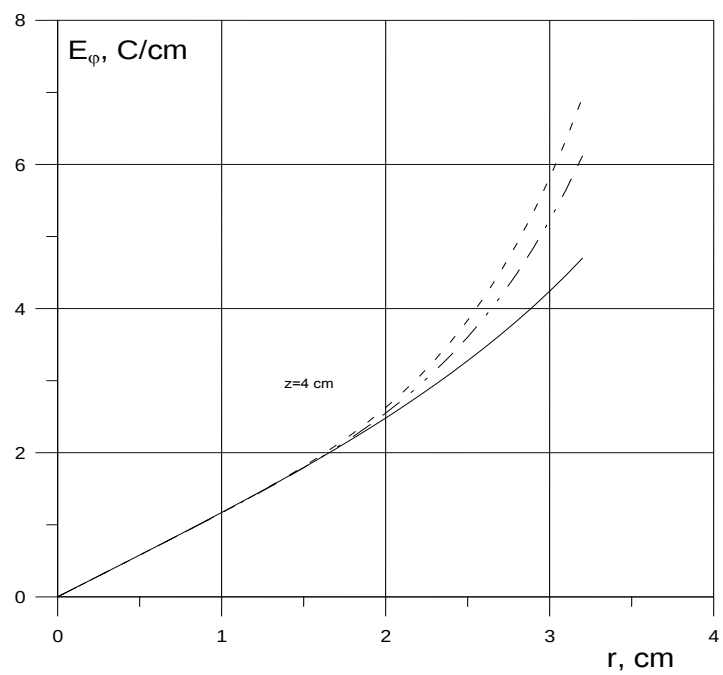

Figure 3. Amplitude of electric curl field inside the plasmoid for z=4cm (the block curve – Thomson's model, dashed-line curve – method of limit relations, pecked line - method of limit relations applied to Thomson's model)

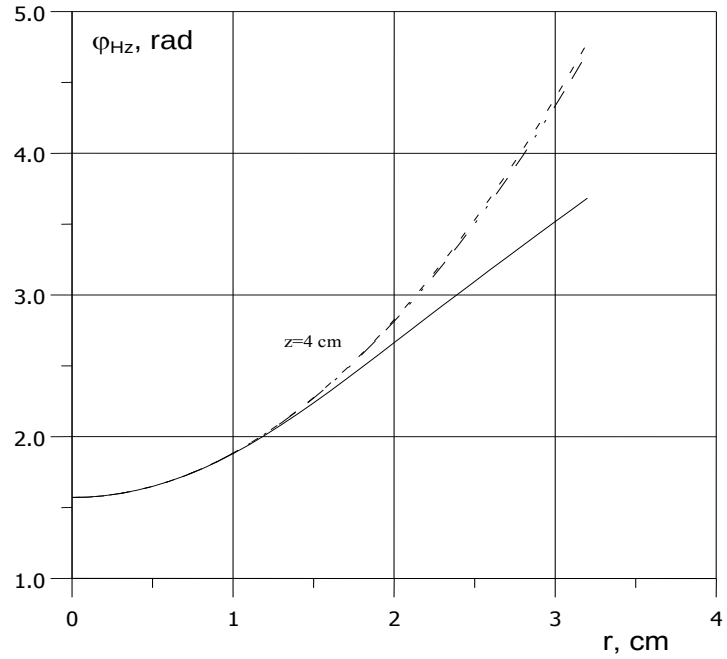

Figure 4. Phase angle of longitudinal component of magnetic field inside the plasmoid for z=4cm (the block curve – Thomson's model, dashed-line curve – method of limit relations, pecked line - method of limit relations applied to Thomson's model)

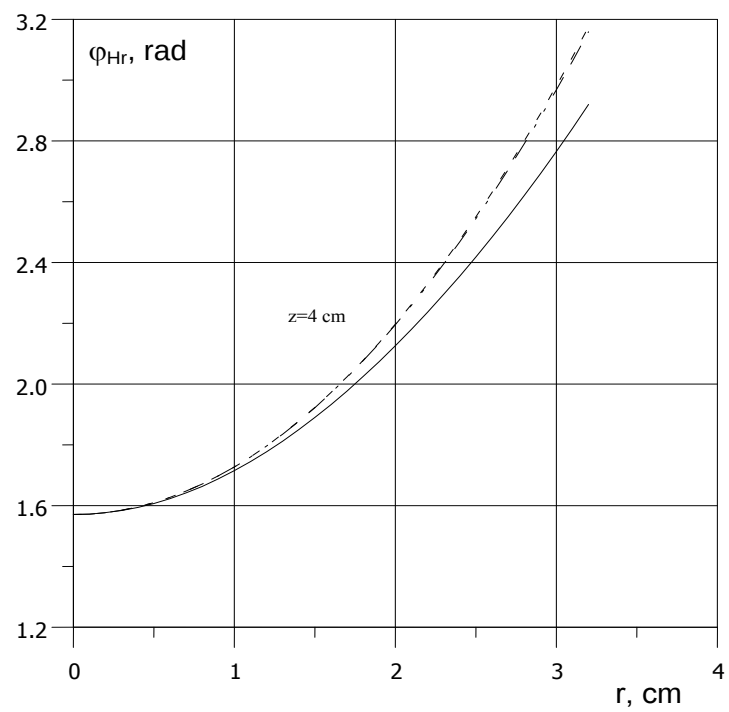

Figure 5. Phase angle of transverse component of magnetic field inside the plasmoid for z=4cm (the block curve – Thomson's model, dashed-line curve – method of limit relations, pecked line - method of limit relations applied to Thomson's model)

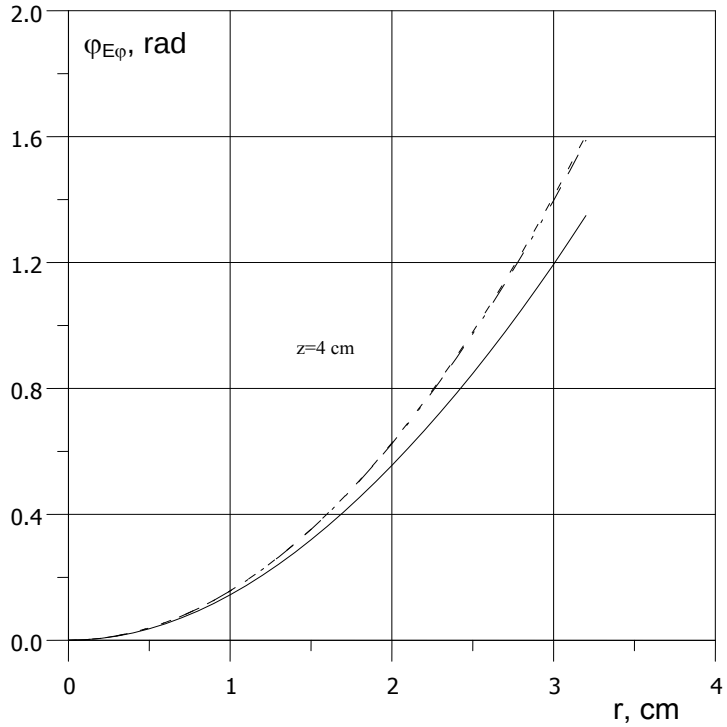

Figure 6. Phase angle of electric curl field inside the plasmoid for z=4cm (the block curve – Thomson's model, dashed-line curve – method of limit relations, pecked line - method of limit relations applied to Thomson's model))

For the purpose of comparison, the curves are also constructed on these graphs, they correspond to the exact solutions of the complete (not simplified for the central range of the plasmoid) equations of Thomson's two-dimensional model of HFI discharge, received in work [7]. The parameters of the real HFI discharge [11, 12], burning in a quartz tube with the diameter of 80 *mm*, the half length of which is L=70 *mm*, and the carrier operation frequency is f=1.76 *MHz* are thus taken as the basis. The discharge is received on the standardized semi-industrial plasma facility HFI 11/60 with the plasma-supporting gas consumption of Q=9 $m^3/hour$. Thus, the complete capacity put into the discharge is about 30 *KW*. As we see, for actual technological units, based on the HF principle of gas induction heating, the method of Maxwell differential equations approximate integration, describing the internal structure of quasistationary electromagnetic fields in the plasma loaded inductor, gives quite exact results in the most interesting, from the point of view of possible applications, near-axial zones of the plasmoid. The obtained system of formulas keeps working efficiency up to the distances of the half of the diameter of plasma bunch luminous area.

In conclusion we will note that the results obtained here, among other things, show the place of the limit relations method among other methods of an approximate integration of differential equations systems with partial derivatives. It takes among them the same place as the pseudospectral method of numerical integration of equations of Burgers type takes among other methods of equations computational solution of incompressible viscous liquid [13].

REFERENCES

1. A. P. Kirpichnikov, "The limit relations for HF inductive discharge" (in Russian) *Izvestia vuzov (News of higher education institutions). Physics*, vol. 36, no. 1, pp. 56-61, Jan. 1993.

2. A. P. Kirpichnikov, "About the limit relations of equation system describing HF quasistationary electromagnetic field HF inductive discharge" (in Russian), *Izvestia vuzov (News of higher education institutions). Physics*, vol. 36, no. 11, pp. 102-103, Nov. 1993.

3. A. P. Kirpichnikov, "About the structure of quasistationary electromagnetic field HF inductive discharge at atmospheric pressure" (in Russian), *Izvestia vuzov (News of higher education institutions). Physics*, vol. 37, no. 2, pp. 77-81, Feb. 1994.

4. A. P. Kirpichnikov, "The structure of quasistationary electromagnetic field of high-frequency inductive discharge near plasma bunch" (in Russian), *Teplofizika Vysokikh Temperatur (High Temperature)*, vol. 33, no. 1, pp. 139-140, Jan.- Feb. 1995.

5. A. P. Kirpichnikov, "About the structure of high-frequency inductive discharge at atmospheric pressure near the plasma bunch axis" (in Russian), *Teplofizika Vysokikh Temperatur (High Temperature)*, vol. 34, no. 6, pp. 989-990, Nov.-Dec. 1996.

6. J. J. Thomson, "The Electrodeless Discharge through Gases", *Philos. Mag*., vol. IV, no. XXV, pp. 1128-1160, Nov. 1927.

7. A. P. Kirpichnikov, "The Thomson's Two-Dimensional Model of High-Frequency Inductive Discharge of the Finite Length", *Journal of Applied Electromagnetism*, vol. 16, no. 1. pp. 12-27, June 2013.

8. A. N. Filatov, *Methods of averaging in differential and integro-differential equations* (in Russian). Tashkent: Fan, 1971.

9. A. N. Filatov, *Asymptotic methods in the theory of differential and integro-differential equations* (in Russian). Tashkent: Fan, 1974.

10. A. V. Gerasimov and A. P. Kirpichnikov, "On the Solution of One Class of Problems of Mathematical Physics", *Journal of Applied Electromagnetism*. vol. 14, no 2, pp. 11-15, Dec. 2012.

11. R. N. Gaynullin, A. R. Gerke and A. P. Kirpichnikov, "Parameter determination of HF induction plasma with regard to the finite inductor length" (in Russian), *Izvestia vuzov (News of higher education institutions). Physics*, vol. 35, no. 6, pp. 122-123, Jun. 1992.

12. R. N. Gaynullin, A. R. Gerke and A. P. Kirpichnikov, "Heat and electromagnetic parameters of high-frequency discharge at the inductive heating of gas" (in Russian), *Engineering and physical magazine (Journal of Engineering Physics and Thermophysics)*, vol. 68, no. 2, pp. 248-252, Mar.-Apr. 1995.

13. R. Peyret and T. D. Taylor, *Computational Methods for Fluid Flow*. New York–Heidelberg-Berlin: Springer-Verlag, 1983.

STUDYING THE EQUATION OF MOTION FOR MAGNETIC FLUIDS WITH NANO-PARTICLE INCLUSIONS (short paper)

Ketevan Kotetishvili*, Elene Iordanishvili**, Natia Kobalia**, Guram Chikhladze**

Georgian Technical University, 0175, 77, M. Kostava str., Tbilisi, Georgia.

* Professor, GTU, Faculty of Informatics & Control Systems,

0177, 20, Chikovani st., Tbilisi, Georgia, ketinooo@hotmail.com

** PhD student, GTU, Faculty of Informatics & Control Systems, 0194, 22, Bakhtrioni st., ap. 45, Tbilisi, Georgia

** PhD student, GTU, Faculty of Informatics & Control Systems, 0197, Temqa, 4 m/d, buil. 9, ap. 181, Tbilisi, Georgia

** Professor, GTU, Faculty of Informatics & Control Systems,

0160, 4a, A. Kazbegi str., ap. 23, Tbilisi, Georgia, gurchix@gmail.com

Abstract

The paper deals with investigations of equation of motion for magnetic fluids, consisting of nano-particles or holding definite nano-particle inclusions. The equation is received by means of application the laws of conservation for linear and angular momentums. In low magnetic fields fluids are unable to reach saturation and nano-particles revolve in additional rotating magnetic field. The magnetization in magnetic fluids increases in spiral form.

When considering the motion of magnetic fluids and mechanical equations for non-compressive magnetic fluid, the application of conservation principles of linear and angular momentum causes the reception of following equations [1] :

$$-\nabla\vec{p}' + \mu_0(\vec{M}\cdot\vec{\nabla})\vec{H} + 2\xi(\vec{\nabla}\times\vec{\omega}) + (\xi+\eta)\vec{\nabla}^2\upsilon = 0, \quad (1)$$

$$T_{mag} + 2\xi\left((\vec{\nabla}\times\vec{\upsilon}) - 2\vec{\omega}\right) = 0, \quad (2)$$

$$p' = p + \rho g y \quad (3)$$

is the modified pressure along the magnetic flux, p is the absolute pressure in Pascal, g being the free falling acceleration along i_y and $\rho -$ the density of the magnetic fluid. ξ is the whirl viscosity of the magnetic fluid, approximately given by $\xi \approx {}^{3\eta\varphi}/_{2}$, $\varphi \ll 1$, η is the viscosity of dynamic shift for the magnetic fluids and $T_{mag} -$

magnetic revolving (whirl) density. For sick signals consider the expression as the sinusoidal and stationary, where the viscosity dominates over conditions of the flux (i.e. the inertia is too small and ignored) and the magnetic fluid reacts only on the force of the revolving momentum and on the density, holding average in time, non-zero components. Again, ignoring the shift in viscosity and the volume coefficients η', λ' we get:

$$T_{mag} = \mu_0(\vec{M} \times \vec{\mathrm{H}}). \tag{4}$$

The law of momentum conservation (ignoring the inertia term) given by (1) includes the terms provided by the pressure and force of weight (first term), by the density of the magnetic force (second term), by the spin-velocity connection (third term) and by the viscosity (fourth term).

As it is seen from (2) the spin-velocity may be considered by two factors: the first – revolving in the flux (whirl flux) provided by $\vec{\nabla} \times \vec{v}$ term and the second $- T_{mag}$, provoked by the magnetic momentum, appearing when the magnetic field and the magnetization in the fluid are not of the same direction any more (are not inter parallel). In the case of absence of the density of the magnetic flux (i.e. for non-magnetic fluids) the equation (2) reduces to the equation of revolving of a momentum, where inertial terms are ignored and the spin-velocity is provoked by revolving in the flux (whirl field) only.

In magnetic fluids, when the flux is absent, the spin-velocity is proportional to the density of the magnetic moment and it actually annihilates differences in measurements of the magnetic field and the magnetization of the field. Averaging the

time, the only remaining non-zero component of the density of the magnetic momentum is given as follows:

$$\langle T_{mag.z}\rangle = \frac{\mu_0}{2} Re\left(\hat{m}_x \hat{h}_y^* - \hat{h}_x \hat{m}_y^*\right), \tag{5}$$

where $\langle \quad \rangle$ denotes the average, while * – complex conjugated.

Taking into account

$$\vec{B} = \mu_0\left(\vec{H} + \vec{M}\right), \tag{6}$$

For time average density of the revolving magnetic momentum and the amplitude of the complex transversal magnetization (5) may be written down as follows:

$$\langle T_{mag.z}\rangle = \frac{1}{2} Re\left(\hat{m}_x \hat{h}_y^* - \mu_0\left(\hat{h}_x + \hat{m}_x\right)\hat{m}_y^*\right) \tag{7}$$

and applying (2), the spin-velocity and the density of the momentum are given by

$$-2\xi \frac{\partial v_x}{\partial y} - 4\xi \omega_x + \langle T_{mag.x}\rangle = 0. \tag{8}$$

Note that the second non-zero term in (1) $\mu_0\left(\vec{M}\cdot\vec{\nabla}\right)\vec{H}$ is the density of the magnetic force F_{mag}, associated with the magnetic fluid. As in figure, field components may vary only along Y-axis, because only non-zero component of the density points in Y-axis direction and, taking into account $\partial B_0/\partial z = 0$ in (6), we get

$$F_{mag,y} = \mu_0\left(m_x \frac{\partial h_y}{\partial x} + m_y \frac{\partial h_y}{\partial y} + \left(\vec{M}_0\right)\frac{\partial h_y}{\partial x}\right), \tag{9}$$

thus

$$F_{mag,y} = \mu_0\left(m_y \frac{\partial h_y}{\partial y}\right) = -\mu_0\left(m_y \frac{\partial m_y}{\partial y}\right),$$

and

$$F_{mag,y} = -\frac{\mu_0}{2}\frac{\partial\left({m_y}^2\right)}{\partial y},$$

and the average value

$$\langle F_{mag,y}\rangle = -\frac{\mu_0}{4}\frac{\partial\left|\hat{m}_y\right|^2}{\partial y}. \tag{10}$$

Here again non-zero, average terms are figured only, and $\widehat{\ }$ symbol represents the complex value of the amplitude of the second signal.

For simplifying (9), the non-zero components of (1) are given by the formulae:

$$-\frac{\partial p'}{\partial x} + 2\xi \frac{\partial \omega_z}{\partial y} + (\xi + \eta) \frac{\partial^2 \upsilon_x}{\partial y^2} = 0, \tag{11}$$

$$-\frac{\partial (p + \rho g y)}{\partial y} - \frac{\mu_0}{4} \frac{\partial \left|\widehat{m}_y(y)\right|^2}{\partial y} = 0, \tag{12}$$

and then follows

$$p(x, y) + \rho g y + \frac{\mu_0}{4} \left|\widehat{m}_y(y)\right|^2 = f(x). \tag{13}$$

Conservation of the momentum gives us the components along i_x and i_y given by (11) and (12), while we have no component along i_z. Assume the pressure may vary due to the length and width of the magnetic flux (i.e. p = p(x, y)) and integrating (12), we arrive to (13), where f(x) is the speed of the flux in X-direction, while dependence of the pressure on free falling acceleration is given by (2) and is dependence on y in m_y. Taking into account the calculations of the magnetic field [2], then

$$\widehat{m}_x = \frac{M_0}{H_0} \frac{\left(j\Omega\tau + 1 + \frac{M_0}{H_0}\right) \hat{h}_x - (\omega_z \tau) \frac{\hat{b}_y}{\mu_0}}{(j\Omega\tau + 1)\left(j\Omega\tau + 1 + \frac{M_0}{H_0}\right) + (\omega_z \tau)^2}, \tag{14}$$

$$\widehat{m}_y = \frac{M_0}{H_0} \frac{(\omega_z \tau) \hat{h}_x + (j\Omega\tau + 1) \frac{\hat{b}_y}{\mu_0}}{(j\Omega\tau + 1)\left(j\Omega\tau + 1 + \frac{M_0}{H_0}\right) + (\omega_z \tau)^2}, \tag{15}$$

$\widehat{m}_x$ and $\widehat{m}_y$ being complex amplitudes depending on spin-velocity ω_z.

Equations (8), (11), (14) and (15) create the closed system for four unknown quantities: spin-velocity ω_z, the speed of the magnetic flux υ_x and two complex amplitudes of the magnetization $\widehat{m}_x$ and $\widehat{m}_y$, directed along i_x and i_y, respectively

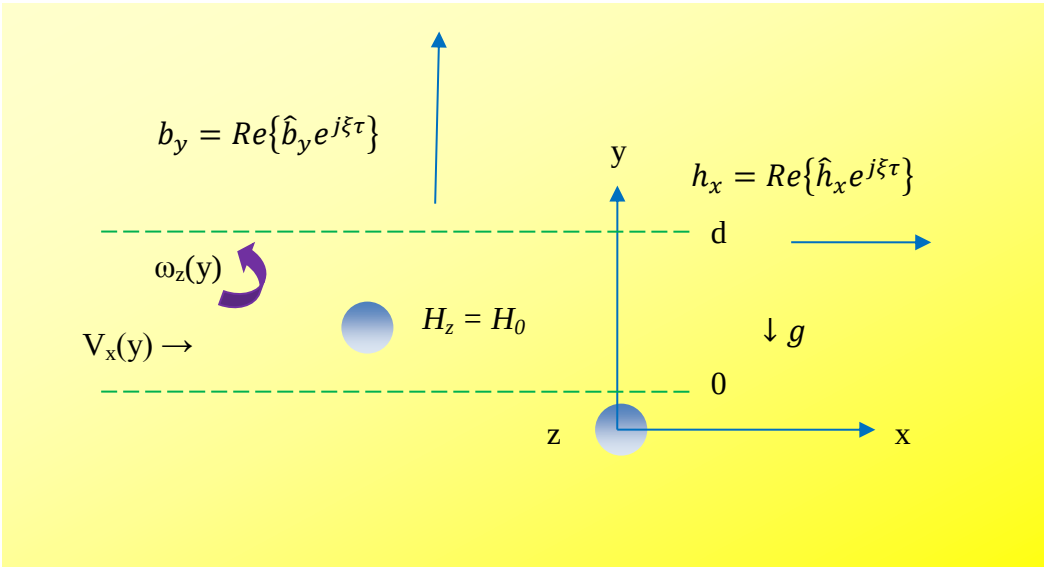

Figure. Magnetic fluid in the vessel with solid, fixed walls (y = 0, and y = d)

Note that $\hat{b}_y$ and $\hat{h}_x$ represent the fields of the sick signal and, thus, are known, while (13) takes into account variations in the pressure of the medium and does not regulate the flux in the medium, although (13) does not take into account measurements of $\langle \hat{m}_y \rangle$ at the variations in the pressure [3,4] .

In the figure the magnetic fluid is presented, located in the vessel with solid, fixed walls (y = 0 and y = d) in the magnetic field H_0, along X-axis the components of the sick signal holding sinusoidal magnetic field with $\hat{h}_x$ complex amplitude and in Y-direction the components of the sick signal magnetic flux density with $\hat{b}_y$ complex amplitude. x and y components of the magnetic field vary in the sinusoidal way with Ω frequency. The speed $v_x(y)$ points in X-direction, the spin-velocity $\omega_z(y)$ points in Z-direction depending only on y coordinate.

REFERENCES

[1]. K.V. Kotetishvili, G.G. Chikhladze. Linearization of the Solution of Langevin's Equation in Magnetic Liquids. Nano Studies, 7, 2013.

[2]. K.V. Kotetishvili, G.G. Chikhladze. The Magnetization Conditions of Modeling of the Action of Magnetic Particles in Magnetic Fluids. JAE. Vol. 16, N. 2, 2014.

[3]. R. Rosensweig. Ferrohydrodynamics. New York, 1997.

[4]. J. Popplewell, R. Rosensweig et al. Magnetic Field Induced Rotations in Ferrofluids. 26. pp. 1852-1854. 1990.

MULTI-HOP DATA TRANSMISSION IN WSN FOR FREE SPACE ENVIRONMENT

Z. Ganev, S. Savov

Department of Electrical Engineering, Technical University of Varna, 9010 Varna, Bulgaria
zganev@gmail.com , sava.savov12@gmail.com

Abstract

This article deals with idealized isotropic model of data transmission in free space environment. This is a model by which data to base station does not arrive directly, but by the means of multi-hop method. Thus data transmission energy is considerably reduced and network life is prolonged , which is a main task of many designer. We have four different examples, which illustrate how the transmission energy can be significantly reduced. The energy model is simulated with Matlab and results visualized with appropriate graphics.

1. INTRODUCTION

It is typical for wireless sensor networks (WSN), that sensor nodes have a limited scope for data transmission. In most cases, packets of information are transmitted from source to receiver, passing through many intermediate nodes. This method allows for the level of energy used to be reduced, but on the other hand imposes the condition of dynamic routing of transmission [2].

Wireless sensor networks are networks with a decentralized structure in which information is wirelessly transmitted, mostly through radio or optical connection and there are high expectations for size and lifetime of the nodes.

Devices compactness and possibility of rapid deployment of WSN makes them extremely suitable for emergency situations: earthquakes, floods, fires and other natural disasters [1]. This network types are preferred when network is of temporary purpose and building infrastructure is difficult or uneconomic.

The so far given characteristics lead to certain requirements: low power consumption (as it works with limited autonomous power supply); small size of sensor nodes; security and protection of data transmitted.

2. ENERGY MODEL

By this model we try to optimize the network. The main goal that we set is to reduce the transmission energy between sensor nodes (SN) and the base station (BS) and with this to have low power consumption of SN. As we know this will prolong the lifetime of our wireless sensor network.

A main challenge in the design of an energy-efficient wireless network is that sending a bit of information through free space directly from node A to node B incurs an energy cost Et, which is a strong function of the distance d between the nodes and can be represented in the following form:

$$E_t = \beta \times d^n \qquad (1)$$

As we can see this is a non-linear function that depends mainly from the distance d (in meters) and path-loss exponent n (a factor that is generally between 2 and 5 and depends on the RF environment). In this formula β is a proportionality constant describing the overhead per bit. Given this greater than linear relationship between energy and distance, using several short intermediate hops (Fig.1) to send a bit is more energy-efficient than using one longer hop [3,4,5,6].

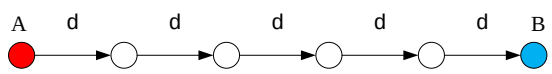

Figure 1. Multi-hop network, using several intermediate nodes to send information

3. RESULTS FROM SIMULATIONS

3.1. Example 1

We assume that n = 2, which is a common case in indoor environments, and β = 0.2 femtojoules/meter. Than one-hop over 50 meters, according (1), requires Et(one-hop) = Et(d=50m) = 0.5 picojoules per bit (Fig. 2).

When we use five-hops of 10 meters (Fig. 3), according (1), require Et(five-hops) = 5 × Et(d=10m) = 5 × 0.02 picojoules per bit = 0.02 picojoules per bit. And we can see this graphically shown in Fig. 4.

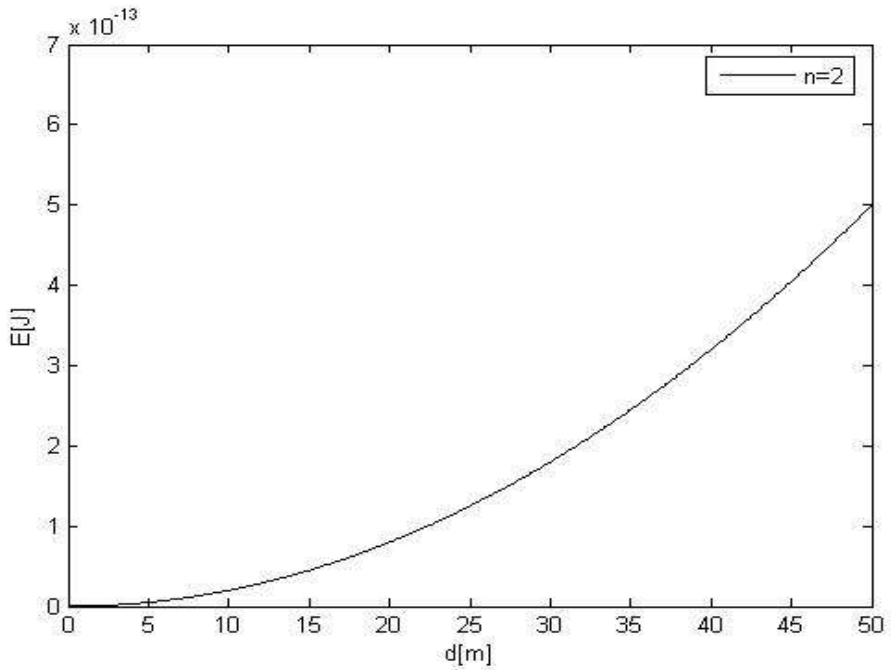

Figure 2.One-hop transmission (d=50m)

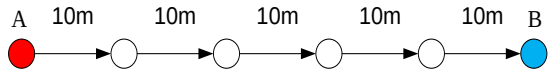

Figure 3. Multi-hop network, using five intermediate hops to send information

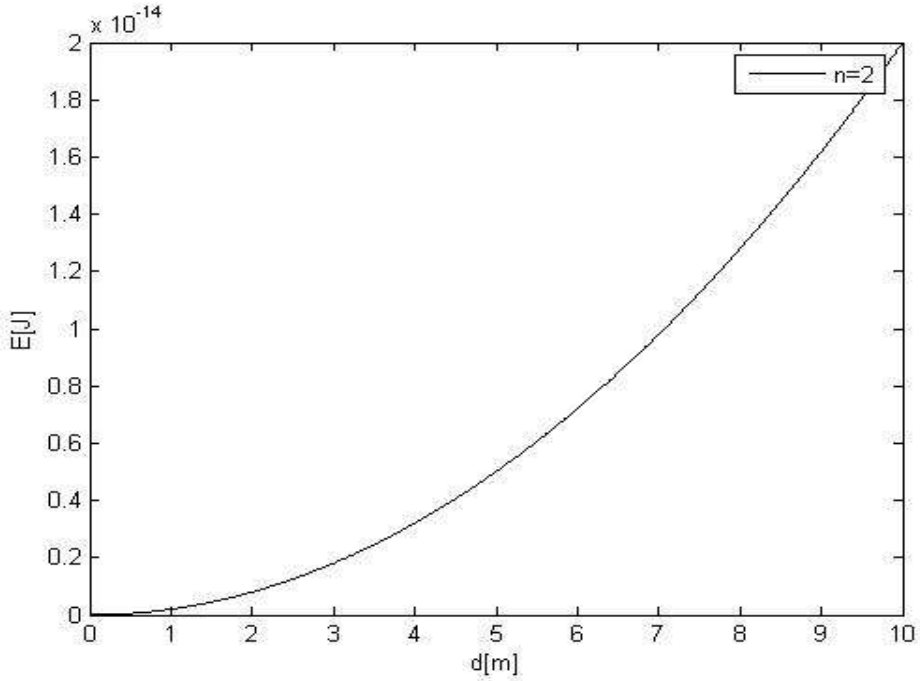

Figure 4.Multi-hop transmission (d=10m)

The multihop approach in this example reduces transmission energy by a factor of 5, (because Et(one-hop) / Et(five-hops) = 5).

3.2. Example 2

We assume that n = 2, which is a common case in indoor environments, and β = 0.2 femtojoules/meter. Than one-hop over 50 meters, according (1), requires Et(one-hop) = Et(d=50m) = 0.5 picojoules per bit (Fig2).

When we use ten-hops of 5 meters (Fig.5), according (1), require only Et(ten-hops) = 10 × Et(d=5m) = 10 × 0.005 picojoules per bit = 0.05 picojoules per bit. And we can see this graphically shown in Figure 6.

Figure 5. Multi-hop network, using ten intermediate hops to send information

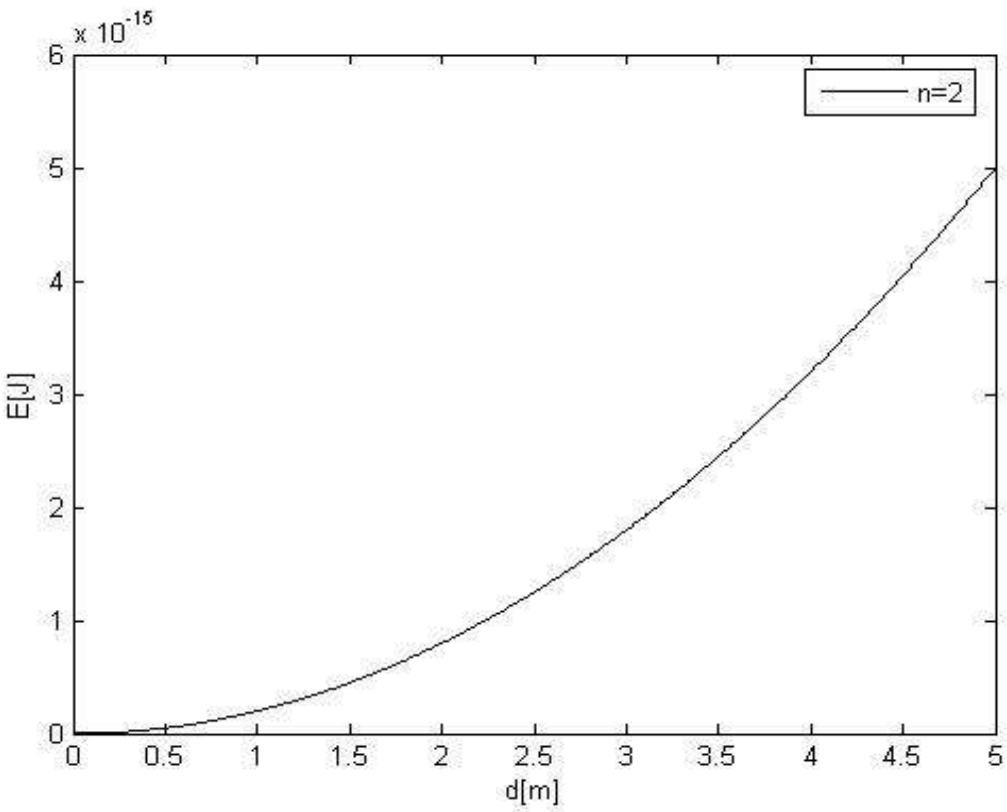

Figure 6.Multi-hop transmission (d=5m)

The multihop approach in this example reduces transmission energy by a factor of 10 (because Et(one-hop) / Et(ten-hops) = 10).

3.3. Example 3

We assume that n = 2, which is a common case in indoor environments, and β = 0.2 femtojoules/meter. Than one-hop over 50 meters, according (1), requires Et(one-hop) = Et(d=50m) = 0.5 picojoules per bit (Fig2).

When we use twenty-five-hops of 2 meters (Fig.7), according (1), require only Et(twenty-five-hops) = 25 × Et(d=2m) = 25 × 0.0008 picojoules per bit = 0.02 picojoules per bit. And we can see this graphically shown in Figure 8.

Figure 7. Multi-hop network, using twenty five intermediate hops to send information

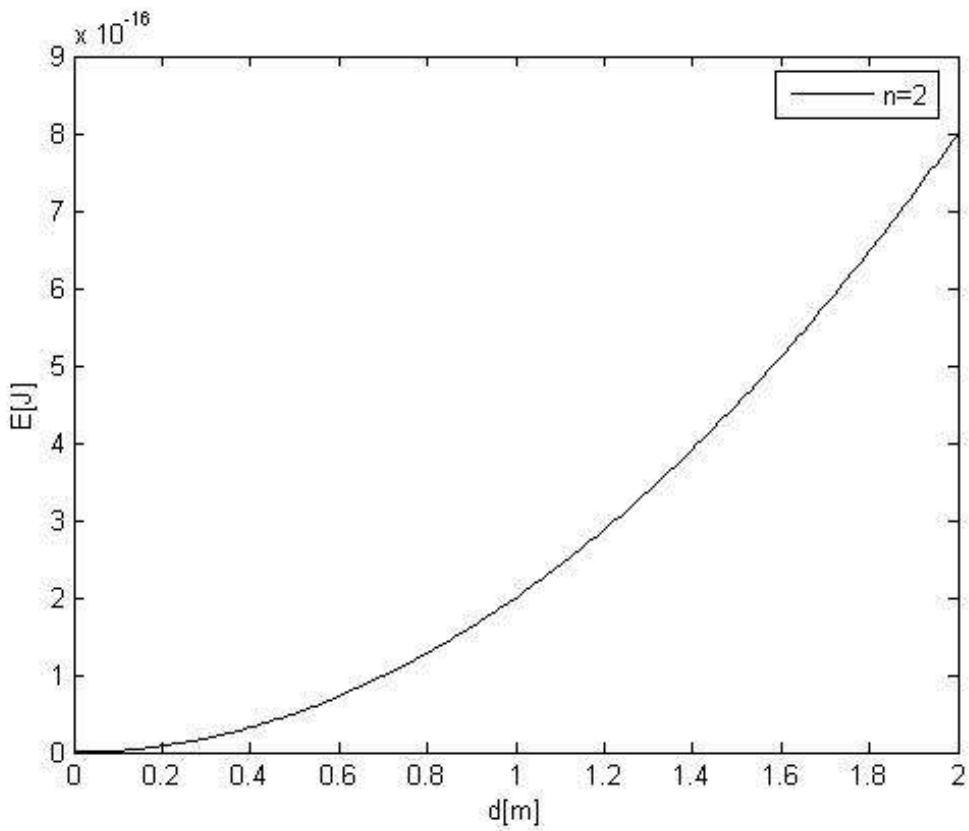

Figure 8.Multi-hop transmission (d=2m)

The multihop approach in this example reduces transmission energy by a factor of 25 (because E_t(one-hop) / E_t(ten-hops) = 25).

3.4. Example 4

We assume that n = 2, which is a common case in indoor environments, and β = 0.2 femtojoules/meter. Than one-hop over 50 meters, according (1), requires Et(one-hop) = Et(d=50m) = 0.5 picojoules per bit (Fig2).

When we use fifty-hops of 1 meter (Fig.9), according (1), require only Et(fifty-hops) = 50 × Et(d=1m) = 50 × 0.0002 picojoules per bit = 0.01 picojoules per bit. We can see this graphically shown in Figure 10.

Figure 9. Multi-hop network, using fifty intermediate hops to send information

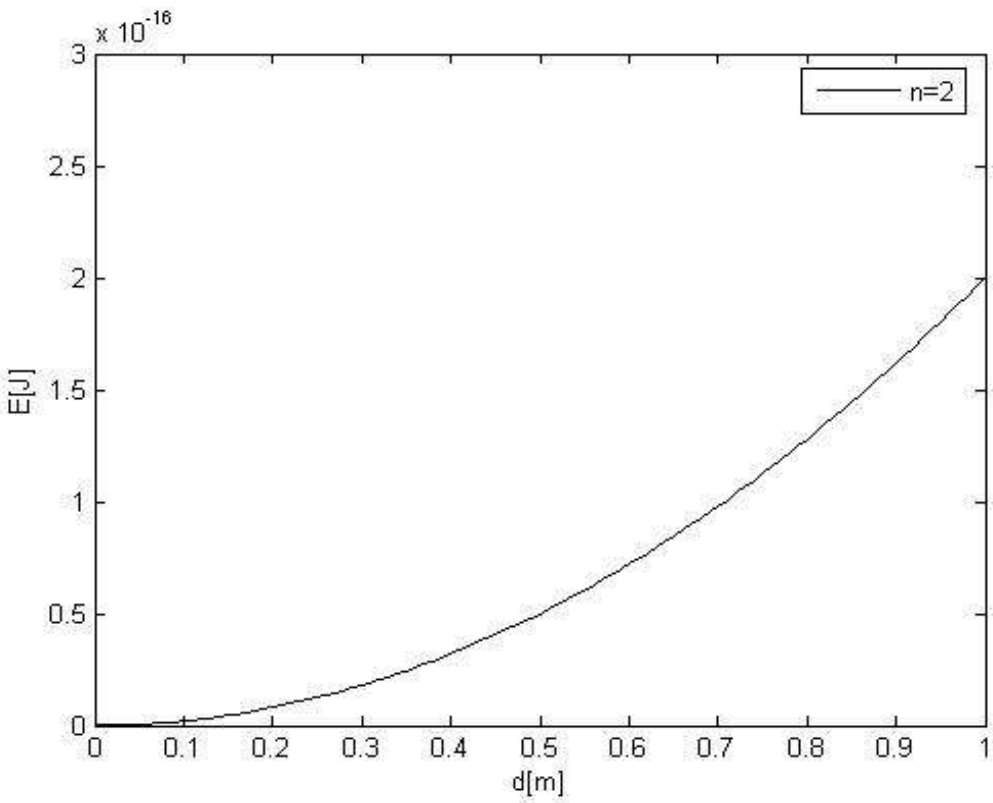

Figure 10.Multi-hop transmission (d=1m)

The multihop approach in this example reduces transmission energy by a factor of 50 (because Et(one-hop) / Et(ten-hops) = 50).

4. CONCLUSION

In this article we present multi-hop model for wireless sensor networks. Multi-hop data transmission in free space environment is examined.

This model does not take into account transmission irregularity, shadowing effects and the energy for calculations. It also does not take into consideration the energy for signal amplification in the different nodes, which are used as active repeaters.

The main purpose was to demonstrate that the energy for transmission of information between two nodes (A and B) can be reduced significantly by using a multi-hop way for communication. It is found through simulations in Matlab environment that the energy transmission is highest in the direct transmission (one-hop) and lowest in the multi-hop approach in example four, where we use 50 hopes. The transmission energy there reduces by a factor of 50 and we have the best efficiency.

REFERENCES

[1] Z.Ganev, S.Savov. "Application of wireless sensor networks", Jubilee Congress of the Technical University of Varna, 2012 (in Bulgarian).

[2] Z.Ganev, Dimova R., "Wireless sensor networks", Annual of Technical University of Varna, Volume 1, pp. 134-138, 2011 (in Bulgarian).

[3] J. L. Gao, *Energy Efficient Routing for Wireless Sensor Networks*, Ph.D. dissertation, University of California, Los Angeles, 2000.

[4] J. M. Rabaey, M. J. Ammer, J. L. Silva, D. Patel & S. Roundy, "PicoRadio supports ad hoc ultra-low power wireless networking", *IEEE Computer*, Vol. 33, July, 2000, pp. 42-48.

[5] Katayoun Sohrabi, *On Low Power Self Organizing Sensor Networks*, Ph. D. thesis, University of California, Los Angeles, 2000.

[6] Karakehayov Z., *Sensor Networks*, Technical University of Sofia (in Bulgarian).